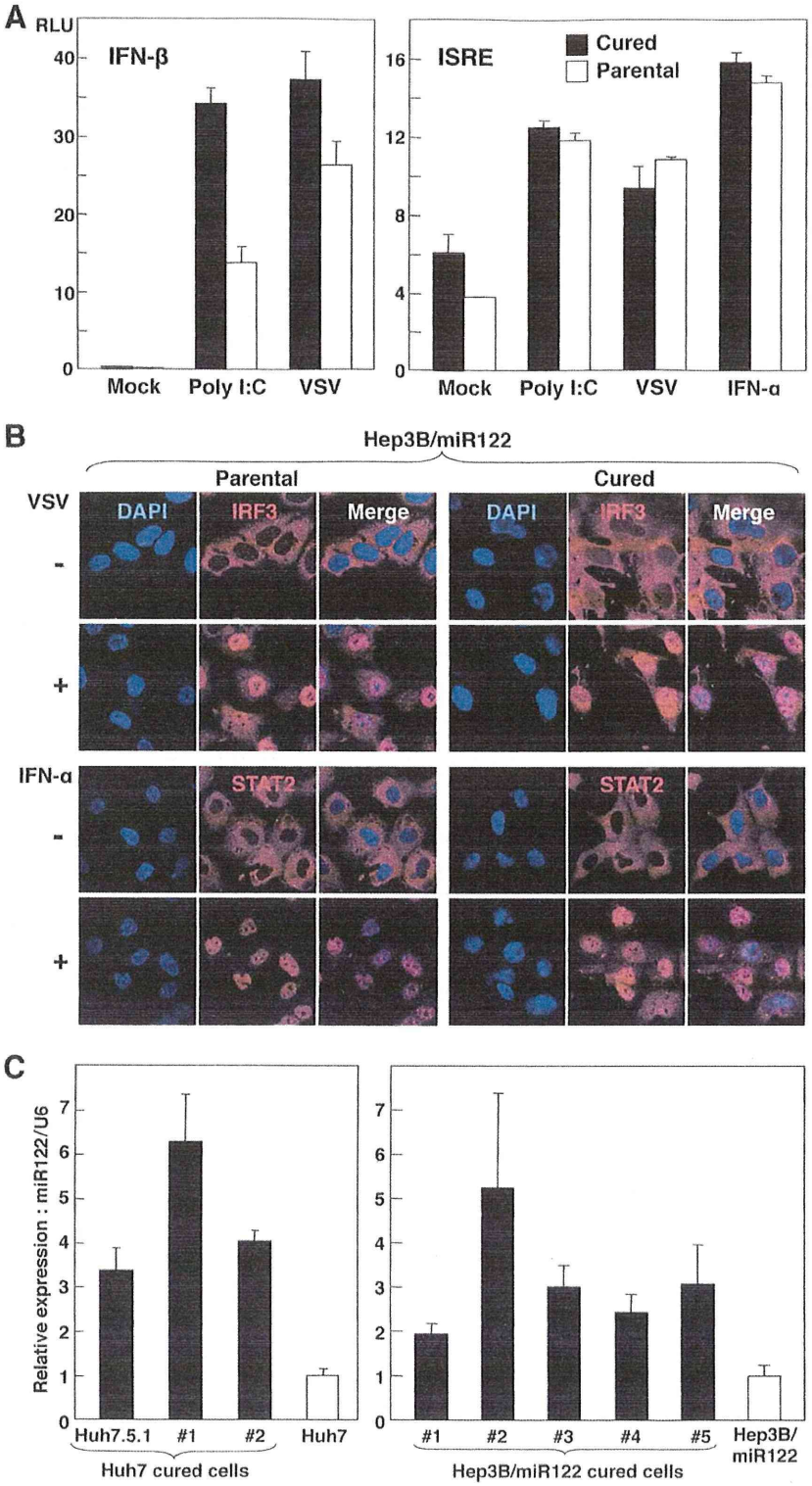

FIG 6 Cured Hep3B/miR122 cells facilitate efficient propagation of HCVcc through enhanced expression of miR122. (A) (Left) Hep3B/miR122 parental cells and cured cells of clone 5 were cotransfected with pIFNβ-Luc and pRL-TK and then infected with the VSV NCP mutant at an MOI of 0.01 or transfected with 1 μg of poly(I·C) at 24 h posttransfection, and luciferase activities were determined at 48 h posttreatment; (right) the cells were cotransfected with pISRE-Luc and pRL-TK and then infected with VSV at an MOI of 0.01 or treated with IFN-α (100 IU/ml) at 24 h posttransfection, and luciferase activities were determined at 48 h posttreatment. (B) (Upper) Hep3B/miR122 parental cells and the cured cells were infected with VSV at an MOI of 0.01, fixed with 4% phosphonoformic acid at 18 h postinfection, and subjected to indirect immunofluorescence assay using rabbit anti-IRF3 antibody, followed by AF488-conjugated anti-rabbit IgG (red); (lower) the cells were treated with IFN-α (100 IU/ml), fixed with 4% paraformaldehyde at 1 h postinfection, and subjected to indirect immunofluorescence assay using rabbit anti-STAT2 antibody, followed by AF488-conjugated anti-rabbit IgG (red). Cell nuclei were stained with 4′,6-diamidino-2-phenylindole (blue). (C) Total RNA was extracted from parental Huh7 and Hep3B/miR122 cells and their cured cells, and the relative expression of miR122 was determined by qRT-PCR by using U6 snRNA as an internal control.

Downloaded from http://jvi.asm.org/ on January 31, 2012 by OSAKA UNIV

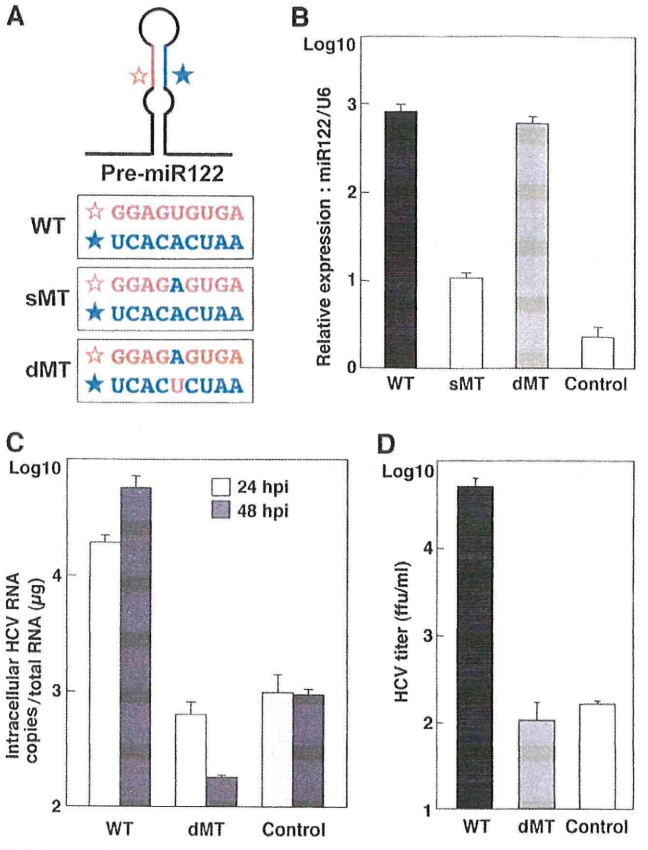

FIG 7 Specific interaction of miR122 with viral RNA is crucial for efficient propagation of HCVcc. (A) Diagram of pre-miR122 and partial nucleotide sequences of wild type (WT) miR122 and mutant miR122 carrying a single mutation (sMT) and double mutations (dMT). (B) Hep3B cells were transduced with lentiviral vectors expressing either WT-, sMT-, or dMT-miR122 or with a control, and the relative expression of miR122 was determined by qRT-PCR by using U6 snRNA as an internal control. (C) Hep3B cells expressing WT- or dMT-miR122 or the control cells were infected with HCVcc at an MOI of 1, and the level of HCV RNA was determined by qRT-PCR at 24 and 48 h postinfection. (D) The culture supernatants were collected at 72 h postinfection, and the viral titers of the supernatants were determined by focus-forming assay using Huh7.5.1 cells.

38, 52). In this study, we assessed the possibility of establishment of human liver cell lines that are susceptible to HCVcc propagation through exogenous expression of miR122 by a lentiviral vector. Although Huh7 cells and their derived cell lines are highly susceptible to propagation of HCVcc, they intrinsically express an abundant amount of miR122. Among the cell lines that we investigated, Hep3B cells exhibit a high sensitivity to HCVcc propagation by expression of miR122 compared to that of Huh7 cells, whereas no sensitivity to HCVcc was observed in the parental Hep3B cells. Therefore, the Hep3B cell line was suggested to be an ideal tool to investigate miR122 function in the life cycle of HCV.

RNA viruses replicate in host cells with high error rates, generating a broad population diversity, which allows rapid adaptation to new environments (33). HCV propagates in the liver of patients with quasispecies heterogeneity and transmits to a new host through contaminated blood or blood products (16). It is known that the complexity of HCV clones significantly decreases during transmission through a genetic bottleneck, resulting in a more homogeneous population. This selection of certain clones is mainly caused by the host factors required for viral replication and immune pressure in a new host and is involved in the early phase of HCV infection in the new environment (18, 25, 32). A sole cell line, Huh7, has been employed in most of the experiments for *in vitro* studies of entry, RNA replication, and particle formation of HCV. Therefore, it has not been possible to assess propagation of HCVcc in human liver cell lines other than Huh7 cells and transmission of HCVcc to liver cell lines of different origins. The establishment of a novel human liver cell line, Hep3B/miR122, for propagation of HCVcc would help to generate new insights into the mutual interaction between HCV and human hepatocytes. Although we are not able to evaluate the effects of the acquired immunity on the induction of the adaptive mutations in cell culture systems, we can assess the host factors involved in the generation of the adaptive mutations by using two different human liver cell lines that support continuous propagation of HCVcc. Further studies are needed to determine the adaptive mutations in the HCV genome by passage in either Hep3B/miR122 or Huh7 cells and in one after the other.

At least seven major HCV genotypes and numerous subtypes have been identified (21), but laboratory strains capable of replicating *in vitro* are limited (36, 64, 68, 70). It is important to establish cell lines that permit the complete propagation of a wide range of HCV genotypes for further understanding of the life cycle of HCV. Although the partial replication of serum-derived HCV in primary hepatocytes in a specialized culture system has been reported (50), development of a simpler and more user-friendly system is required for promotion of research on HCV. It might be feasible to establish new cell culture systems for not only various genotypes of infectious HCV clones but also serum-derived HCV by the expression of miR122 in various human liver cell lines.

While preparing the manuscript, Narbus et al. reported that the expression of miR122 enhances HCV replication in HepG2/CD81 cells (46). Our data also demonstrated that the expression of miR122 increased HCV replication in HepG2/CD81 cells, as shown in Fig. 1D. However, the impact of miR122 expression on the production of infectious particles in HepG2/CD81 cells is significantly lower than that in Huh7 cells (46). Although LH86 (71) and Li23 (30) cell lines derived from human hepatocellular carcinoma have been shown to permit propagation of HCVcc, these cell lines are not well characterized. In contrast, the Hep3B cell line has been utilized in a wide range of research fields for a long time, resulting in the accumulation of many sources of data from genomic and proteomic analyses (1, 47, 55, 63, 67). Moreover, the Hep3B cell line is available from the major cell banks all over the world, which should readily allow reevaluation of the findings in this study. Comparison of the experimental data on HCVcc propagation between Huh7 and Hep3B/miR122 cells might provide a clue to understanding the host factors crucial for the efficient propagation of HCV in human liver cells.

The higher susceptibility to HCVcc propagation of the cured cells derived from Huh7 cells than the parental cells was suggested to be attributable to impairment of the innate immune response (57). However, this is not the only reason for efficient propagation of HCVcc in the Huh7-based cured cell lines (17). It has been shown that cured cell lines, such as Huh7.5.1 and Huh7-Lunet, express a higher level of miR122 than the parental Huh7 cells (13), suggesting that upregulation of miR122 in the cured cells participates in the efficient propagation of HCVcc. However, the level of

Downloaded from http://jvi.asm.org/ on January 31, 2012 by OSAKA UNIV

miR122 expression in the cured Hep3B cells was not necessarily correlated with the replication efficiency of HCVcc in the present work (Fig. 6C). Most recently, Denard et al. reported that the expression of CREB3L1/OASIS, which specifically prevents division of virus-infected cells, in cured Huh7 cells was reduced compared to that in the parental cells (12), suggesting that CREB3L1/OASIS is also involved in the enhancement of HCVcc propagation in the cured cells.

In this study, we have shown that expression of miR122 confers susceptibility to human liver cell lines for the efficient propagation of HCVcc. Elimination of the HCV genome from the replicon cells of Hep3B/miR122 cells enhanced propagation of HCVcc in accord with the increment of miR122 expression, and propagation of HCVcc in the cured cells was continuously increased in every passage. Furthermore, the interaction between HCV RNA and miR122 was shown to be specific for production of infectious particles in Hep3B/miR122 cells. The establishment of a new permissive cell line for HCVcc allows us not only to investigate the biological function of miR122 on the life cycle of HCV but also to develop novel therapeutics for chronic hepatitis C.

ACKNOWLEDGMENTS

We thank M. Tomiyama for her secretarial work. We also thank M. Hijikata, T. Wakita, F. Chisari, T. Kawai, S. Akira, and M. Whitt for providing experimental materials.

This work was supported in part by grants-in-aid from the Ministry of Health, Labor, and Welfare (Research on Hepatitis); the Ministry of Education, Culture, Sports, Science, and Technology; and the Osaka University Global Center of Excellence Program.

REFERENCES

1. Aden DP, Fogel A, Plotkin S, Damjanov I, Knowles BB. 1979. Controlled synthesis of HBsAg in a differentiated human liver carcinoma-derived cell line. Nature 282:615–616.
2. Bai S, et al. 2009. MicroRNA-122 inhibits tumorigenic properties of hepatocellular carcinoma cells and sensitizes these cells to sorafenib. J. Biol. Chem. 284:32015–32027.
3. Bartel DP. 2009. MicroRNAs: target recognition and regulatory functions. Cell 136:215–233.
4. Blight KJ, McKeating JA, Rice CM. 2002. Highly permissive cell lines for subgenomic and genomic hepatitis C virus RNA replication. J. Virol. 76: 13001–13014.
5. Burns DM, D'Ambrogio A, Nottrott S, Richter JD. 2011. CPEB and two poly(A) polymerases control miR-122 stability and p53 mRNA translation. Nature 473:105–108.
6. Castoldi M, et al. 2011. The liver-specific microRNA miR-122 controls systemic iron homeostasis in mice. J. Clin. Invest. 121:1386–1396.
7. Chang J, et al. 2008. Liver-specific microRNA miR-122 enhances the replication of hepatitis C virus in nonhepatic cells. J. Virol. 82:8215–8223.
8. Chang J, et al. 2004. miR-122, a mammalian liver-specific microRNA, is processed from hcr mRNA and may downregulate the high affinity cationic amino acid transporter CAT-1. RNA Biol. 1:106–113.
9. Chang KS, Jiang J, Cai Z, Luo G. 2007. Human apolipoprotein E is required for infectivity and production of hepatitis C virus in cell culture. J. Virol. 81:13783–13793.
10. Cormier EG, et al. 2004. CD81 is an entry coreceptor for hepatitis C virus. Proc. Natl. Acad. Sci. U. S. A. 101:7270–7274.
11. Date T, et al. 2004. Genotype 2a hepatitis C virus subgenomic replicon can replicate in HepG2 and IMY-N9 cells. J. Biol. Chem. 279: 22371–22376.
12. Denard B, et al. 2011. The membrane-bound transcription factor CREB3L1 is activated in response to virus infection to inhibit proliferation of virus-infected cells. Cell Host Microbe 10:65–74.
13. Ehrhardt M, et al. 18 April 2011. Profound differences of microRNA expression patterns in hepatocytes and hepatoma cell lines commonly used in hepatitis C virus studies. Hepatology. [Epub ahead of print.]
14. Elmen J, et al. 2008. LNA-mediated microRNA silencing in non-human primates. Nature 452:896–899.
15. Evans MJ, et al. 2007. Claudin-1 is a hepatitis C virus co-receptor required for a late step in entry. Nature 446:801–805.
16. Farci P, et al. 2000. The outcome of acute hepatitis C predicted by the evolution of the viral quasispecies. Science 288:339–344.
17. Feigelstock DA, Mihalik KB, Kaplan G, Feinstone SM. 2010. Increased susceptibility of Huh7 cells to HCV replication does not require mutations in RIG-I. Virol. J. 7:44.
18. Feliu A, Gay E, Garcia-Retortillo M, Saiz JC, Forns X. 2004. Evolution of hepatitis C virus quasispecies immediately following liver transplantation. Liver Transpl. 10:1131–1139.
19. Ge D, et al. 2009. Genetic variation in IL28B predicts hepatitis C treatment-induced viral clearance. Nature 461:399–401.
20. Gentzsch J, et al. 2011. Hepatitis C virus complete life cycle screen for identification of small molecules with pro- or antiviral activity. Antiviral Res. 89:136–148.
21. Gottwein JM, et al. 2009. Development and characterization of hepatitis C virus genotype 1-7 cell culture systems: role of CD81 and scavenger receptor class B type I and effect of antiviral drugs. Hepatology 49: 364–377.
22. Haid S, Windisch MP, Bartenschlager R, Pietschmann T. 2010. Mouse-specific residues of claudin-1 limit hepatitis C virus genotype 2a infection in a human hepatocyte cell line. J. Virol. 84:964–975.
23. Henke JI, et al. 2008. microRNA-122 stimulates translation of hepatitis C virus RNA. EMBO J. 27:3300–3310.
24. Herker E, et al. 2010. Efficient hepatitis C virus particle formation requires diacylglycerol acyltransferase-1. Nat. Med. 16:1295–1298.
25. Hughes MG, Jr, et al. 2005. HCV infection of the transplanted liver: changing CD81 and HVR1 variants immediately after liver transplantation. Am. J. Transplant. 5:2504–2513.
26. Huntzinger E, Izaurralde E. 2011. Gene silencing by microRNAs: contributions of translational repression and mRNA decay. Nat. Rev. Genet. 12:99–110.
27. Jangra RK, Yi M, Lemon SM. 2010. Regulation of hepatitis C virus translation and infectious virus production by the microRNA miR-122. J. Virol. 84:6615–6625.
28. Jopling CL, Schutz S, Sarnow P. 2008. Position-dependent function for a tandem microRNA miR-122-binding site located in the hepatitis C virus RNA genome. Cell Host Microbe 4:77–85.
29. Jopling CL, Yi M, Lancaster AM, Lemon SM, Sarnow P. 2005. Modulation of hepatitis C virus RNA abundance by a liver-specific microRNA. Science 309:1577–1581.
30. Kato N, et al. 2009. Efficient replication systems for hepatitis C virus using a new human hepatoma cell line. Virus Res. 146:41–50.
31. Lanford RE, et al. 2010. Therapeutic silencing of microRNA-122 in primates with chronic hepatitis C virus infection. Science 327:198–201.
32. Laskus T, et al. 2004. Analysis of hepatitis C virus quasispecies transmission and evolution in patients infected through blood transfusion. Gastroenterology 127:764–776.
33. Lauring AS, Andino R. 2010. Quasispecies theory and the behavior of RNA viruses. PLoS Pathog. 6:e1001005.
34. Lavanchy D. 2009. The global burden of hepatitis C. Liver Int. 29(Suppl. 1):74–81.
35. Lin LT, et al. 2010. Replication of subgenomic hepatitis C virus replicons in mouse fibroblasts is facilitated by deletion of interferon regulatory factor 3 and expression of liver-specific microRNA 122. J. Virol. 84: 9170–9180.
36. Lindenbach BD, et al. 2005. Complete replication of hepatitis C virus in cell culture. Science 309:623–626.
37. Lohmann V, et al. 1999. Replication of subgenomic hepatitis C virus RNAs in a hepatoma cell line. Science 285:110–113.
38. Machlin ES, Sarnow P, Sagan SM. 2011. Masking the 5′ terminal nucleotides of the hepatitis C virus genome by an unconventional microRNA-target RNA complex. Proc. Natl. Acad. Sci. U. S. A. 108:3193–3198.
39. Masaki T, et al. 2010. Production of infectious hepatitis C virus by using RNA polymerase I-mediated transcription. J. Virol. 84:5824–5835.
40. Miyanari Y, et al. 2007. The lipid droplet is an important organelle for hepatitis C virus production. Nat. Cell Biol. 9:1089–1097.
41. Moradpour D, Penin F, Rice CM. 2007. Replication of hepatitis C virus. Nat. Rev. Microbiol. 5:453–463.
42. Moriishi K, Matsuura Y. 2007. Evaluation systems for anti-HCV drugs. Adv. Drug Deliv. Rev. 59:1213–1221.

Downloaded from http://jvi.asm.org/ on January 31, 2012 by OSAKA UNIV

43. **Moriishi K, Matsuura Y.** 2007. Host factors involved in the replication of hepatitis C virus. Rev. Med. Virol. 17:343–354.
44. **Moriishi K, Matsuura Y.** 2003. Mechanisms of hepatitis C virus infection. Antivir. Chem. Chemother. 14:285–297.
45. **Moriishi K, et al.** 2010. Involvement of PA28gamma in the propagation of hepatitis C virus. Hepatology 52:411–420.
46. **Narbus CM, et al.** 2011. HepG2 cells expressing microRNA miR-122 support the entire hepatitis C virus life cycle. J. Virol. 85:12087–12092.
47. **Park JG, et al.** 1995. Characterization of cell lines established from human hepatocellular carcinoma. Int. J. Cancer 62:276–282.
48. **Pileri P, et al.** 1998. Binding of hepatitis C virus to CD81. Science 282: 938–941.
49. **Ploss A, et al.** 2009. Human occludin is a hepatitis C virus entry factor required for infection of mouse cells. Nature 457:882–886.
50. **Ploss A, et al.** 2010. Persistent hepatitis C virus infection in microscale primary human hepatocyte cultures. Proc. Natl. Acad. Sci. U. S. A. 107: 3141–3145.
51. **Randall G, et al.** 2007. Cellular cofactors affecting hepatitis C virus infection and replication. Proc. Natl. Acad. Sci. U. S. A. 104:12884–12889.
52. **Roberts AP, Lewis AP, Jopling CL.** 2011. miR-122 activates hepatitis C virus translation by a specialized mechanism requiring particular RNA components. Nucleic Acids Res. 39:7716–7729.
53. **Russell RS, et al.** 2008. Advantages of a single-cycle production assay to study cell culture-adaptive mutations of hepatitis C virus. Proc. Natl. Acad. Sci. U. S. A. 105:4370–4375.
54. **Scarselli E, et al.** 2002. The human scavenger receptor class B type I is a novel candidate receptor for the hepatitis C virus. EMBO J. 21:5017–5025.
55. **Seow TK, Liang RC, Leow CK, Chung MC.** 2001. Hepatocellular carcinoma: from bedside to proteomics. Proteomics 1:1249–1263.
56. **Skalsky RL, Cullen BR.** 2010. Viruses, microRNAs, and host interactions. Annu. Rev. Microbiol. 64:123–141.
57. **Sumpter R, Jr, et al.** 2005. Regulating intracellular antiviral defense and permissiveness to hepatitis C virus RNA replication through a cellular RNA helicase, RIG-I. J. Virol. 79:2689–2699.
58. **Suppiah V, et al.** 2009. IL28B is associated with response to chronic hepatitis C interferon-alpha and ribavirin therapy. Nat. Genet. 41: 1100–1104.
59. **Tanaka Y, et al.** 2009. Genome-wide association of IL28B with response to pegylated interferon-alpha and ribavirin therapy for chronic hepatitis C. Nat. Genet. 41:1105–1109.
60. **Tani H, et al.** 2007. Replication-competent recombinant vesicular stomatitis virus encoding hepatitis C virus envelope proteins. J. Virol. 81: 8601–8612.
61. **Targett-Adams P, Boulant S, McLauchlan J.** 2008. Visualization of double-stranded RNA in cells supporting hepatitis C virus RNA replication. J. Virol. 82:2182–2195.
62. **Thomas DL, et al.** 2009. Genetic variation in IL28B and spontaneous clearance of hepatitis C virus. Nature 461:798–801.
63. **Vannucchi AM, et al.** 1993. Effects of cyclosporin A on erythropoietin production by the human Hep3B hepatoma cell line. Blood 82:978–984.
64. **Wakita T, et al.** 2005. Production of infectious hepatitis C virus in tissue culture from a cloned viral genome. Nat. Med. 11:791–796.
65. **Walters KA, et al.** 2006. Host-specific response to HCV infection in the chimeric SCID-beige/Alb-uPA mouse model: role of the innate antiviral immune response. PLoS Pathog. 2:e59.
66. **Windisch MP, et al.** 2005. Dissecting the interferon-induced inhibition of hepatitis C virus replication by using a novel host cell line. J. Virol. 79: 13778–13793.
67. **Wong N, et al.** 2005. Transcriptional profiling identifies gene expression changes associated with IFN-alpha tolerance in hepatitis C-related hepatocellular carcinoma cells. Clin. Cancer Res. 11:1319–1326.
68. **Yi M, Villanueva RA, Thomas DL, Wakita T, Lemon SM.** 2006. Production of infectious genotype 1a hepatitis C virus (Hutchinson strain) in cultured human hepatoma cells. Proc. Natl. Acad. Sci. U. S. A. 103: 2310–2315.
69. **Yoneyama M, et al.** 2004. The RNA helicase RIG-I has an essential function in double-stranded RNA-induced innate antiviral responses. Nat. Immunol. 5:730–737.
70. **Zhong J, et al.** 2005. Robust hepatitis C virus infection in vitro. Proc. Natl. Acad. Sci. U. S. A. 102:9294–9299.
71. **Zhu H, et al.** 2007. Hepatitis C virus triggers apoptosis of a newly developed hepatoma cell line through antiviral defense system. Gastroenterology 133:1649–1659.

Downloaded from http://jvi.asm.org/ on January 31, 2012 by OSAKA UNIV

JOURNAL OF VIROLOGY, Dec. 2011, p. 13185–13194 Vol. 85, No. 24
0022-538X/11/$12.00 doi:10.1128/JVI.06099-11
Copyright © 2011, American Society for Microbiology. All Rights Reserved.

Dysfunction of Autophagy Participates in Vacuole Formation and Cell Death in Cells Replicating Hepatitis C Virus▽§

Shuhei Taguwa,[1]† Hiroto Kambara,[1]† Naonobu Fujita,[2] Takeshi Noda,[2] Tamotsu Yoshimori,[2] Kazuhiko Koike,[3] Kohji Moriishi,[4] and Yoshiharu Matsuura[1]*

Department of Molecular Virology, Research Institute for Microbial Diseases,[1] and Department of Genetics, Graduate School of Medicine,[2] Osaka University, Osaka 565-0871, Department of Gastroenterology, Graduate School of Medicine, University of Tokyo, Tokyo 113-8655,[3] and Department of Microbiology, Faculty of Medicine, Yamanashi University, Yamanashi 409-3898,[4] Japan

Received 22 August 2011/Accepted 4 October 2011

Hepatitis C virus (HCV) is a major cause of chronic liver diseases. A high risk of chronicity is the major concern of HCV infection, since chronic HCV infection often leads to liver cirrhosis and hepatocellular carcinoma. Infection with the HCV genotype 1 in particular is considered a clinical risk factor for the development of hepatocellular carcinoma, although the molecular mechanisms of the pathogenesis are largely unknown. Autophagy is involved in the degradation of cellular organelles and the elimination of invasive microorganisms. In addition, disruption of autophagy often leads to several protein deposition diseases. Although recent reports suggest that HCV exploits the autophagy pathway for viral propagation, the biological significance of the autophagy to the life cycle of HCV is still uncertain. Here, we show that replication of HCV RNA induces autophagy to inhibit cell death. Cells harboring an HCV replicon RNA of genotype 1b strain Con1 but not of genotype 2a strain JFH1 exhibited an incomplete acidification of the autolysosome due to a lysosomal defect, leading to the enhanced secretion of immature cathepsin B. The suppression of autophagy in the Con1 HCV replicon cells induced severe cytoplasmic vacuolation and cell death. These results suggest that HCV harnesses autophagy to circumvent the harmful vacuole formation and to maintain a persistent infection. These findings reveal a unique survival strategy of HCV and provide new insights into the genotype-specific pathogenicity of HCV.

Hepatitis C virus (HCV) is a major causative agent of bloodborne hepatitis and currently infects at least 180 million people worldwide (58). The majority of individuals infected with HCV develop chronic hepatitis, which eventually leads to liver cirrhosis and hepatocellular carcinoma (25, 48). In addition, HCV infection is known to induce extrahepatic diseases such as type 2 diabetes and malignant lymphoma (20). It is believed that the frequency of development of these diseases varies among viral genotypes (14, 51). However, the precise mechanism of the genotype-dependent outcome of HCV-related diseases has not yet been elucidated. Despite HCV's status as a major public health problem, the current therapy with pegylated interferon and ribavirin is effective in only around 50% of patients with genotype 1, which is the most common genotype worldwide, and no effective vaccines for HCV are available (35, 52). Although recently approved protease inhibitors for HCV exhibited a potent antiviral efficacy in patients with genotype 1 (36, 43), the emergence of drug-resistant mutants is a growing problem (16). Therefore, it is important to clarify the life cycle and pathogenesis of HCV for the development of more potent remedies for chronic hepatitis C.

* Corresponding author. Mailing address: Department of Molecular Virology, Research Institute for Microbial Diseases, Osaka University, 3-1, Yamadaoka, Suita-shi, Osaka 565-0871, Japan. Phone: 81-6-6879-8340. Fax: 81-6-6879-8269. E-mail: matsuura@biken.osaka-u.ac.jp.
† These authors contributed equally to this work.
§ Supplemental material for this article may be found at http://jvi.asm.org/.
▽ Published ahead of print on 12 October 2011.

HCV belongs to the genus *Hepacivirus* of the family *Flaviviridae* and possesses a single positive-stranded RNA genome with a nucleotide length of 9.6 kb, which encodes a single polyprotein consisting of approximately 3,000 amino acids (40). The precursor polyprotein is processed by host and viral proteases into structural and nonstructural (NS) proteins (34). Not only viral proteins but also several host factors are required for efficient replication of the HCV genome, where NS5A is known to recruit various host proteins and to form replication complexes with other NS proteins (39). In the HCV-propagating cell, host intracellular membranes are reconstructed for the viral niche known as the membranous web, where it is thought that progeny viral RNA and proteins are concentrated for efficient replication and are protected from defensive degradation, as are the host protease and nucleases (38).

Autophagy is a bulk degradation process, wherein portions of cytoplasm and organelles are enclosed by a unique membrane structure called an autophagosome, which subsequently fuses with the lysosome for degradation (37, 60). Autophagy occurs not only in order to recycle amino acids during starvation but also to clear away deteriorated proteins or organelles irrespective of nutritional stress. In fact, the deficiency of autophagy leads to the accumulation of disordered proteins that can ultimately cause a diverse range of diseases, including neurodegeneration and liver injury (12, 29, 30), and often to type 2 diabetes and malignant lymphoma (9, 32).

Recently, it has been shown that autophagy is provoked upon replication of several RNA viruses and is closely related to their propagation and/or pathogenesis. Coxsackievirus B3

Downloaded from http://jvi.asm.org/ on November 21, 2011 by Yoshiharu Matsuura

utilizes autophagic membrane as a site of genome replication, whereas influenza virus attenuates apoptosis through the induction of autophagy (10, 59). Moreover, several groups have reported that HCV induces autophagy for infection or replication (5, 49); however, the role(s) of autophagy in the propagation of HCV is still controversial and the involvement of autophagy in the pathogenesis of HCV has not yet been clarified. In this study, we examined the biological significance of the autophagy observed in cells in which the HCV genome replicates.

MATERIALS AND METHODS

Plasmids. The plasmids pmStrawberry-C1, pmStrawberry-Atg4B^{C74A}, pmRFP-GFP-LC3, pEGFP-LC3, and pEGFP-Atg16L were described previously (7, 8, 24). The plasmids pFGR-JFH1 and pSGR-JFH1 were kind gifts from T. Wakita.

Cell culture. All cell lines were cultured at 37°C under a humidified atmosphere with 5% CO_2. Huh7 cells were cultivated in Dulbecco's modified Eagle's medium (DMEM) supplemented with 10% fetal bovine serum (FBS), nonessential amino acids, 100 U/ml penicillin, and 100 mg/ml streptomycin. For the starvation, the cells were cultivated with Earle's balanced salt solution (EBSS) (Sigma) for 6 h. HCV replicon cells were established as described previously (53). The plasmid pairs pFK-I$_{389}$ neo/NS3-3′/NK5.1 and pFK-I$_{389}$ neo/FGR/NK5.1 and pFGR-JFH1 and pSGR-JFH1 were linearized with ScaI or XbaI. The plasmids pFGR-JFH1 and pSGR-JFH1 were treated with mung bean exonuclease. The linearized DNA was transcribed *in vitro* by using the MEGAscript T7 kit (Applied Biosystems) according to the manufacturer's protocol. The transcribed RNA was electroporated into cells under conditions of 270 V and 960 mF using a Gene Pulser (Bio-Rad). All HCV replicon cells were maintained in DMEM containing 10% FBS, nonessential amino acids, and 1 mg/ml G418 (Nacalai).

Reagents and antibodies. Concanamycin A and bafilomycin A1 were purchased from Sigma and Fluka, respectively. E64D and pepstatin A were from Peptide Institute Inc. Rabbit anti-HCV NS5A polyclonal antibody was described previously (45). Mouse monoclonal anti-JEV NS3 antibody was prepared by immunization using the recombinant protein spanning amino acid residues 171 to 619 of JEV NS3. Rabbit polyclonal anti-LC3 (PM036), mouse monoclonal anti-RFP (8D6), and anti-62/SQSTM1 (5F2) antibodies were purchased from Medical & Biological Laboratories. Rabbit polyclonal anti-cathepsin B (FL-339) and mouse monoclonal anti-LAMP1 (H4A3) antibodies were from Santa Cruz Biotechnology. Mouse monoclonal anti-HCV NS5A (HCM-131-5), rabbit polyclonal anti-β-actin, and mouse monoclonal anti-Golgin97 (CDF4) antibodies were from Austral Biologicals, Sigma, and Invitrogen, respectively. Mouse monoclonal and rabbit polyclonal anti-cathepsin B antibodies were from Calbiochem. Mouse monoclonal anti-p62/SQSTM1 (5F2) and anti-ATP6V0D1 (ab56441) antibodies were from Abcam. Rabbit polyclonal anti-Atg4B antibody was from Sigma. Mouse anti-double-stranded RNA (dsRNA) IgG2a (J2 and K1) antibodies were from Biocenter Ltd. (Szirak, Hungary).

Transfection, infection, and immunoblotting. Transfection and infection were carried out as described previously (53). Each lysosome-enriched fraction was isolated by using the Lysosome Enrichment Kit for Tissue and Cultured Cells (Pierce) according to the manufacturer's protocol. Samples were subjected to 12.5% sodium dodecyl sulfate-polyacrylamide gel electrophoresis. The proteins were transferred to polyvinylidene difluoride membranes (Millipore) and were reacted with the appropriate antibodies. The immune complexes were visualized with Super Signal West Femto substrate (Pierce) and detected by an LAS-3000 image analyzer system (Fujifilm). The protein bands of LC3 and β-actin were quantified by Multi Gauge software (Fujifilm), and the values of LC3 were normalized to those of β-actin.

Fluorescence microscopy. Cells were cultured on glass slides and then fixed with 4% paraformaldehyde in phosphate-buffered saline (PBS) at room temperature for 30 min. After being washed twice with PBS, the cells were permeabilized at room temperature for 20 min with PBS containing 0.25% saponin and then blocked with PBS containing 0.2% gelatin (gelatin-PBS) for 60 min at room temperature. The cells were incubated with gelatin-PBS containing appropriate antibodies at 37°C for 60 min and washed three times with PBS containing 1% Tween 20 (PBST). The resulting cells were incubated with gelatin-PBS containing corresponding fluorescent-conjugated secondary antibodies at 37°C for 60 min and then washed three times with PBST. The stained cells were covered with Vectashield mounting medium containing DAPI (4′,6-diamidino-2-phenylindole) (Vector Laboratories Inc.) and observed with a FluoView FV1000 laser scanning confocal microscope (Olympus). Time-lapse video microscopy was performed at 37°C with a DeltaVision microscope system (Applied Precision Inc.) equipped with a ΔTC3 culture dish system (Bioptechs) for temperature control.

Quantification of pro-cathepsin B. Each cell line was seeded on 12-well type I collagen-coated dishes (IWAKI) and cultured for 48 h. The supernatant and the cells were harvested and subjected to quantification of pro-cathepsin B by using Quantikine human pro-cathepsin B immunoassay (R&D Systems) according to the manufacturer's protocol.

Statistical analysis. Estimated values were represented as the means ± standard deviations. The significance of differences in the means was determined by Student's *t* test.

RESULTS

Autophagy is induced in the HCV replicating cell in a strain-dependent manner. To determine whether autophagy is induced during the replication of HCV, we investigated the phosphoethanolamine (PE) conjugation of LC3 in HCV replicon cells in which HCV RNA was autonomously replicating. As shown in Fig. 1A, the amounts of PE-conjugated LC-3 (LC3-II), a conventional marker for an autophagosomal membrane, in Huh7 cells were slightly increased by starvation, in conjunction with a reduction of the unmodified LC-3 (LC3-I). In contrast, the amount of LC3-II was significantly increased in the subgenomic and full genomic HCV replicon cells of the genotype 1b strain Con1 (SGR^{Con1} and FGR^{Con1}), whereas a small amount of LC3-II was detected in the full genomic replicon cells of the genotype 2a strain JFH1 (FGR^{JFH1}). We also examined the subcellular localization of LC3 by using confocal microscopy. Although LC3 was diffusely detected in the cytoplasm of naïve Huh7 cells, small foci of the accumulated LC3 appeared after starvation (Fig. 1B), whereas many LC3 foci that were larger in size than those in the starved cells appeared in the cytoplasm, particularly near the nucleus, in both SGR^{Con1} and FGR^{Con1} cells. However, a low level of LC3 focus formation comparable to that in the starved cells was observed in the FGR^{JFH1} cells. Most of the LC3 foci were not colocalized with NS5A, an HCV protein of the viral replication complex, in the HCV replicon cells, as reported previously (49). Elimination of HCV RNA from the SGR^{Con1} cells by treatment with alpha interferon (SGR^{cured}) abrogated the lipidation and accumulation of LC3 (Fig. 1C and D). Interestingly, overexpression of the HCV polyprotein of genotype 1b by an expression plasmid induced no autophagy (data not shown), suggesting that replication of viral RNA is required for induction of autophagy. Furthermore, neither lipidation nor accumulation of LC3 was observed in SGR^{JEV} cells harboring subgenomic replicon RNA cells of Japanese encephalitis virus (JEV), which is also a member of the family *Flaviviridae* (Fig. 1C and D). These results suggest that replication of HCV but not that of JEV induces autophagy.

The autophagy flux is impaired in the replicon cells of HCV strain Con1 after a step of autophagosome formation. To further examine the autophagy induced in the HCV replicon cells in more detail, Huh7 and SGR^{Con1} cells were treated with pepstatin A and E64D, inhibitors of aspartic protease and cysteine protease, respectively. In this assay, treatment of intact cells capable of inducing autophagy with the inhibitors increases the amount of LC3-II, whereas no increase is observed in cells impaired in the autophagic degradation. The amount of LC3-II was significantly increased in the naïve Huh7

Downloaded from http://jvi.asm.org/ on November 21, 2011 by Yoshiharu Matsuura

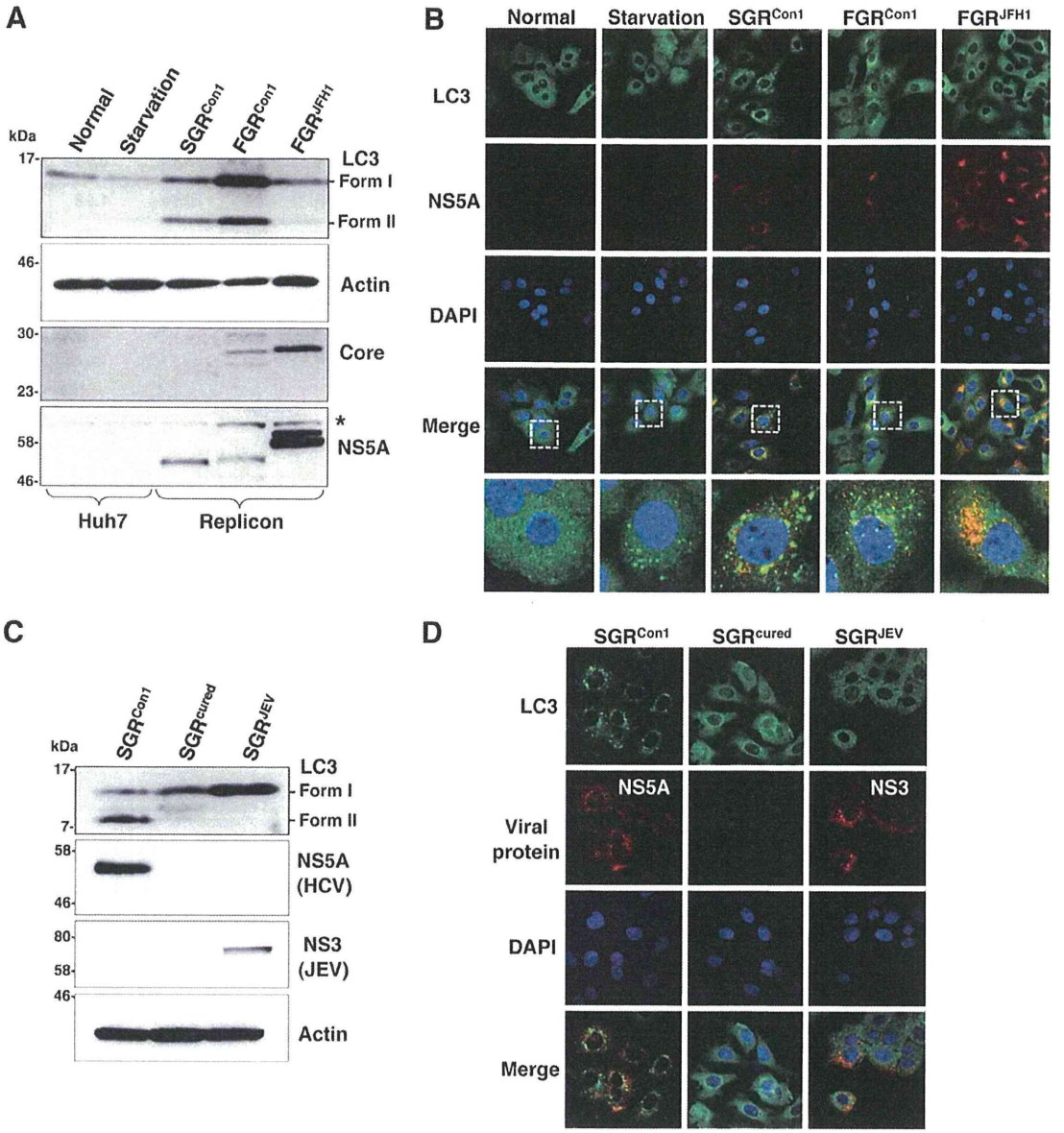

FIG. 1. Induction of autophagy in the HCV replicon cells. (A) The starved Huh7 cells and HCV replicon cells harboring a sub- or full genomic RNA of strain Con1 or strain JFH1 were subjected to immunoblotting using the appropriate antibodies. The asterisk indicates a nonspecific band. (B) Subcellular localizations of LC3 and NS5A were determined by confocal microscopy. The replicon cells and the starved Huh7 cells were stained with DAPI and then reacted with rabbit polyclonal anti-LC3 and mouse monoclonal anti-NS5A antibodies, respectively, followed by Alexa Fluor 488- and 594-conjugated secondary antibodies, respectively. The boxed areas in the merged images are magnified. (C) SGR^{Con1} cells were treated with alpha interferon for 1 week to remove the HCV replicon RNA. The resulting cells were designated SGR^{cured} cells. The SGR^{Con1}, SGR^{cured}, and SGR^{JEV} cells were lysed and subjected to immunoblotting using the appropriate antibodies. (D) Subcellular localization of LC3 and JEV NS3 and HCV NS5A was determined by confocal microscopy after staining with DAPI, followed by staining with rabbit polyclonal anti-LC3 and anti-JEV NS3 antibodies and mouse monoclonal anti-NS5A antibodies and then with the appropriate secondary antibodies. The data shown are representative of three independent experiments.

cells by treatment with the inhibitors, whereas only a slight increase was observed in the SGR^{Con1} cells (5.4-fold versus 1.6-fold) (Fig. 2A), suggesting that autophagy is suppressed in the HCV replicon cells. Furthermore, cytoplasmic accumulation of LC3 was significantly increased in the naïve Huh7 cells by treatment with the inhibitors, in contrast to the only slight increase induced by treatment in the SGR^{Con1} cells (Fig. 2B). In SGR^{Con1} cells, the LC3 foci were colocalized with the polyubiquitin-binding protein p62/SQSTM1, a specific substrate for autophagy (18), suggesting that most of the autophagosomes were distributed in the cytoplasm of the SGR^{Con1} cells (Fig. 2B and C). Next, to examine the autophagy flux in the SGR^{Con1} cells, we monitored the green fluorescent protein (GFP)-conjugated LC3 dynamics in living cells by using time-lapse imaging techniques (see movies in the supplemental material). A large number of small GFP-LC3 foci were detected in the

Downloaded from http://jvi.asm.org/ on November 21, 2011 by Yoshiharu Matsuura

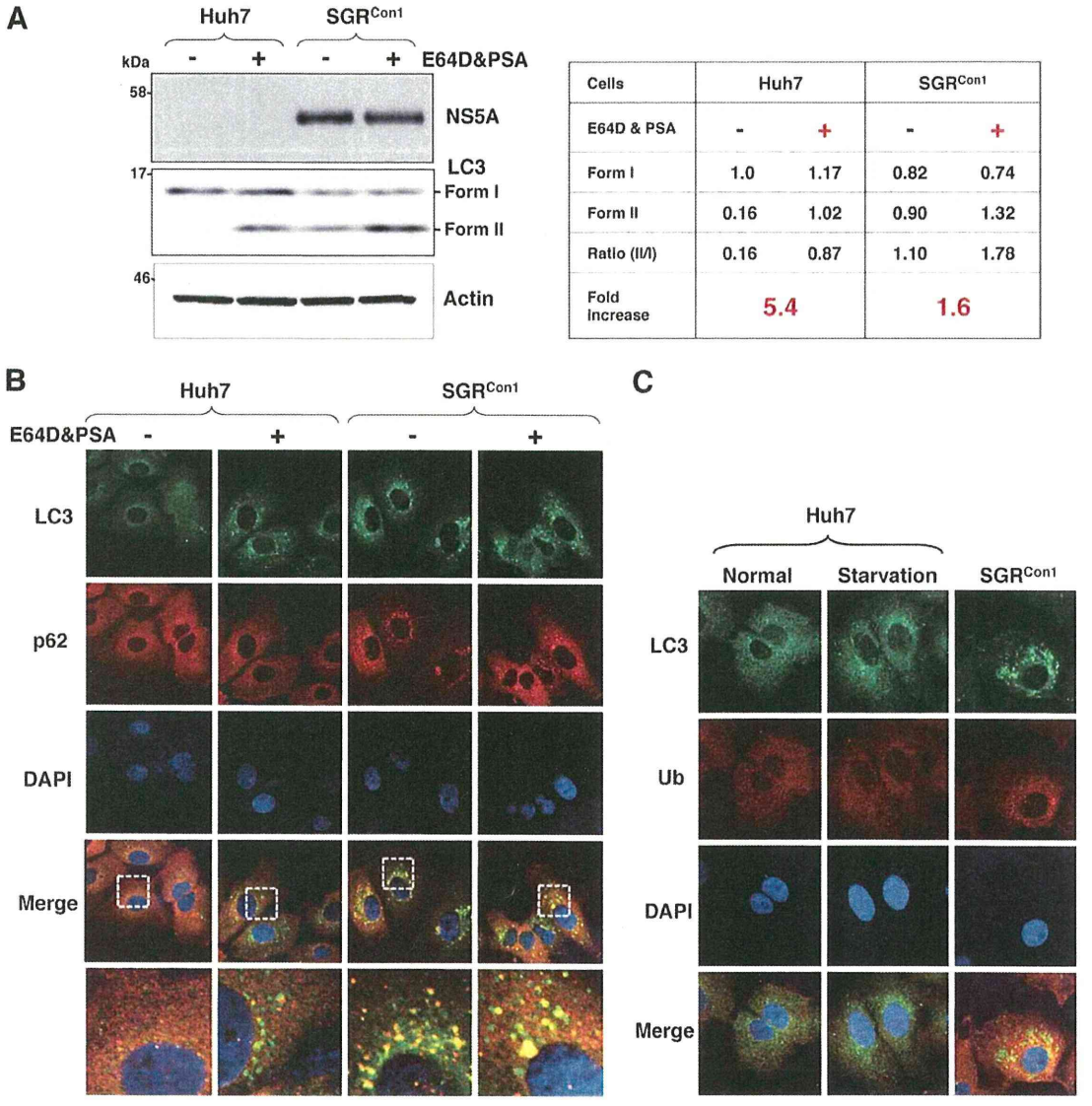

Cells	Huh7		SGR^{Con1}	
E64D & PSA	-	+	-	+
Form I	1.0	1.17	0.82	0.74
Form II	0.16	1.02	0.90	1.32
Ratio (II/I)	0.16	0.87	1.10	1.78
Fold Increase	5.4		1.6	

FIG. 2. Autophagy flux is impaired in the HCV replicon cells. Autophagy flux assay using lysosomal protease inhibitors. (A) Huh7 and SGR^{Con1} cells were treated with 20 μM E64D and pepstatin A (PSA) for 6 h, and the cell lysates were subjected to immunoblotting. The density of the protein band was estimated by Multi Gauge version 2.2 (Fujifilm). (B) After nuclear staining with DAPI, the intracellular localizations of LC3 and p62 in each cell were determined by staining with rabbit polyclonal anti-LC3 and mouse monoclonal anti-62 antibodies, respectively, followed by staining with Alexa Fluor 488- and 594-conjugated secondary antibodies, respectively. The resulting cells were observed by confocal microscopy. (C) Colocalization of accumulated LC3 with ubiquitinated proteins (Ub) in SGR^{Con1} cells. Nontreated and starved Huh7 cells and SGR^{Con1} cells were fixed and stained with DAPI and rabbit anti-LC3 and anti-ubiquitin (6C1.17) (BD) polyclonal antibodies, respectively, and then with the appropriate secondary antibodies. Subcellular localizations of LC3 and Ub were determined by confocal microscopy. The data shown are representative of three independent experiments.

starved Huh7 cell, moved quickly, and finally disappeared within 30 min. Although small foci of GFP-LC3 exhibited characteristics similar to those in the starved cells, some large foci exhibited confined movement and maintained constant fluorescence for at least 3 h in the SGR^{Con1} cells. The GFP-LC3 foci in the SGR^{JFH1} cells showed characteristics similar to those in the starved cells. These results support the notion that autophagy flux is suppressed in the SGR^{Con1} cells at some step after autophagosome formation.

Impairment of autolysosomal acidification causes incomplete autophagy in the replicon cell of strain Con1. Recent studies have shown that some viruses inhibit the autophagy pathway by blocking the autolysosome formation (10, 42). Therefore, we determined the autolysosome formation in the HCV replicon cells through the fusion of autophagosome with lysosome. Colocalization of small foci of LC3 with LAMP1, a lysosome marker, was observed in the starved Huh7 cells, SGR^{Con1} cells, and SGR^{JFH1} cells but not in the SGR^{cured} cells (Fig. 3A), suggesting that autolysosomes are formed in the HCV replicon cells of both Con1 and JFH1 strains. The autolysosome is acidified by the vacuolar-type H^+ ATPase (V-ATPase) and degrades substrates by the lysosomal acidic hy-

Downloaded from http://jvi.asm.org/ on November 21, 2011 by Yoshiharu Matsuura

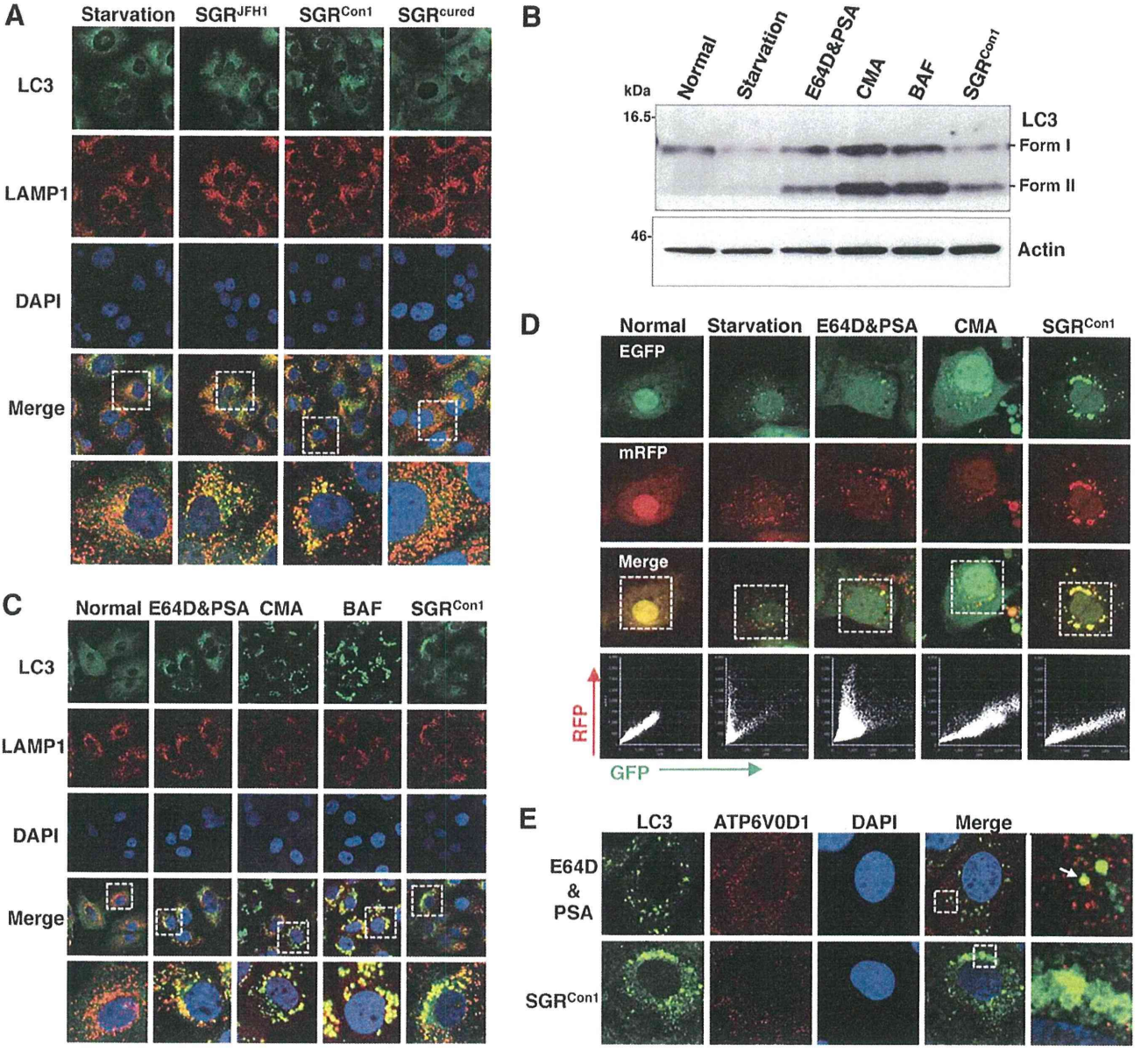

FIG. 3. Inhibition of autophagy maturation in HCV replicon cells. (A) After nuclear staining with DAPI, starved Huh7 cells, replicon cells, and SGR^{cured} cells were stained with rabbit polyclonal anti-LC3 and mouse monoclonal anti-LAMP1 antibodies followed by Alexa Fluor 488- and 594-conjugated secondary antibodies, respectively, and examined by confocal microscopy. The boxed regions in the merged images are magnified. (B and C) Huh7 cells were treated with 20 μM protease inhibitors (E64D and PSA) or a 20 nM concentration of a V-ATPase inhibitor (CMA or BAF) for 6 h. (B) Cell lysates were subjected to immunoblotting using antibodies against LC3 and β-actin. (C) Intracellular localization of LAMP1 and LC3 was determined by confocal microscopy after staining with DAPI and appropriate antibodies. The boxed areas in the merged images are magnified. (D) Tandem fluorescence-tagged LC3 assay. The expression plasmid encoding mRFP-GFP-tandem-tagged LC3 was transfected into naïve and starved Huh7 cells or into the SGR^{Con1} cells treated with the indicated inhibitors at 36 h posttransfection. The resulting cells were fixed at 42 h posttransfection, and the relative GFP and RFP signals were determined by confocal microscopy. The fluorescent values in the boxes of the merged images were determined and shown as dot plots in the bottom column of the grid, in which the *x* and *y* axes indicate the signals of GFP and RFP, respectively. (E) Huh7 cells treated with E64D and PSA and the SGR^{Con1} cells were stained with DAPI and then with rabbit polyclonal anti-LC3 and mouse monoclonal anti-ATP6V0D1 antibodies followed by Alexa Fluor 488- and 594-conjugated secondary antibodies, respectively. The boxed regions in the merged images are magnified. A white arrow indicates colocalization of LC3 and ATP6V0D1. The data shown are representative of three independent experiments.

drolases in the vesicle (2). Next, to determine the possibility of a deficiency in the acidification of the autolysosome on the autophagic dysfunction in the Con1 replicon cells, Huh7 cells were treated with the protease inhibitors E64D and pepstatin A (PSA) or with each of the V-ATPase inhibitors concanamycin A (CMA) and bafilomycin A1 (BAF). The amount of LC3-II was significantly increased in Huh7 cells treated with the inhibitors just as in the SGR^{Con1} cells (Fig. 3B). Further-

Downloaded from http://jvi.asm.org/ on November 21, 2011 by Yoshiharu Matsuura

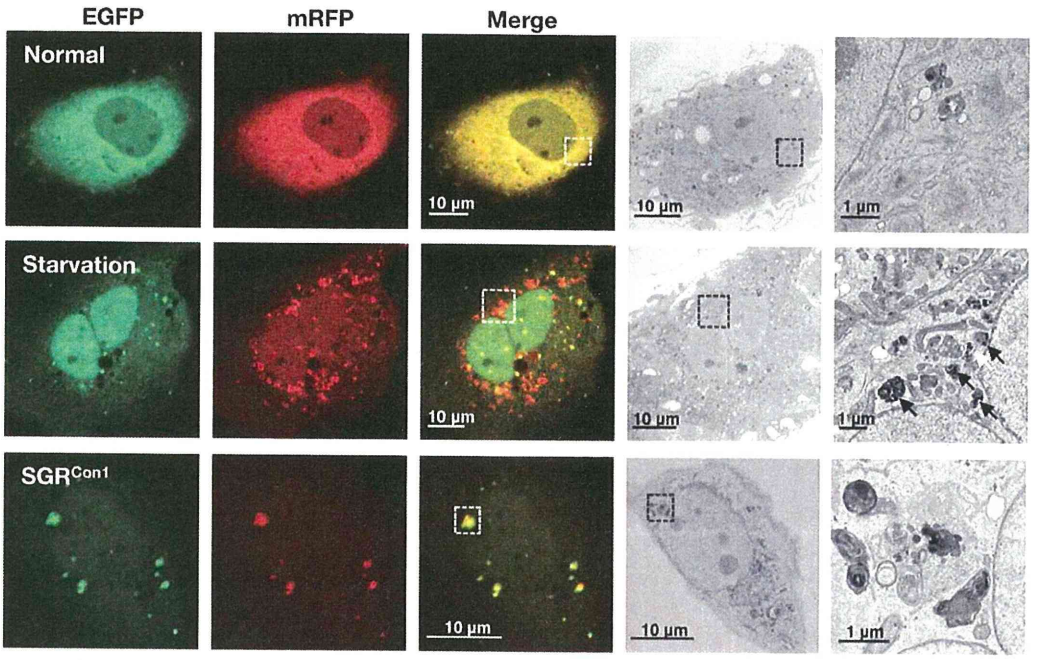

FIG. 4. Correlative fluorescence microscopy-electron microscopy (FM-EM) analysis. The expression plasmid encoding mRFP-GFP-tandem-tagged LC3 was transfected into naïve and starved Huh7 cells or into the SGR^{Con1} cells as described in the legend to Fig. 3D, and the mRFP-GFP-tandem-tagged LC3 signals were observed at 36 h posttransfection. The boxed regions in the merged images are magnified. The data shown are representative of three independent experiments.

more, the large foci of LC3 colocalized with LAMP1 appeared in the cells treated with the V-ATPase inhibitors, as seen in SGR^{Con1} cells (Fig. 3C). These results suggest that stacked autophagosome flux caused by the inhibition of lysosomal degradation or acidification exhibits characteristics similar to those observed in the Con1 replicon cells.

Since the fluorescence of GFP but not that of monomeric red fluorescent protein (mRFP) disappears under the acidic environment, expression of mRFP-GFP tandem fluorescent-tagged LC3 (tfLC3) is capable of being used to monitor the acidic status of the autolysosome (24). Both GFP and mRFP fluorescent signals were unfused, some of them accumulated as small foci in Huh7 cells after starvation or by treatment with the protease inhibitors, and half of the foci of mRFP were not colocalized with those of GFP (Fig. 3D), indicating that half of the foci are in an acidic state due to maturation into an autolysosome after fusion with a lysosome. On the other hand, the large foci of GFP and mRFP were completely colocalized in Huh7 cells treated with CMA or in the SGR^{Con1} cells. These results suggest that the large foci of LC3 in the SGR^{Con1} cells are not under acidic conditions. Recently, it was shown that the lack of lysosomal acidification in human genetic disorders due to dysfunction in assembly/sorting of V-ATPase induces incomplete autophagy similar to that observed in SGR^{Con1} cells (31, 45). Therefore, to explore the reason for the lack of acidification of the autolysosome in the SGR^{Con1} cells, we examined the subcellular localization of ATP6V0D1, a subunit of the integral membrane V_0 complex of V-ATPase. Colocalization of ATP6V0D1 with large foci of LC3 was observed in Huh7 cells treated with the protease inhibitors but not in SGR^{Con1} cells (Fig. 3E), suggesting that dislocation of V-ATPase may participate in the impairment of the autolysosomal acidification in the SGR^{Con1} cells.

We further examined the morphological characteristics of the LC3-positive compartments by using correlative fluorescence microscopy-electron microscopy (FM-EM) (Fig. 4). The starved Huh7 cells exhibited a small double-membrane vesicle (white arrow) and high-density single-membrane structures (black arrows) in close proximity to the correlative position of the GFP- and mRFP-positive LC3 compartments, which are considered to be the autophagosome and lysosome/autolysosome, respectively. In contrast, many high-density membranous structures were detected in the correlative position of the large GFP- and mRFP-positive LC3 compartment in the SGR^{Con1} cells, which is well consistent with the observation in the time-lapse imaging in which small foci of LC3 headed toward and assembled with the large LC3-positive compartment (see movies in the supplemental material). These results suggest that the formation of large aggregates with aberrant inner structures in the SGR^{Con1} cells may impair maturation of the autolysosome through the interference of further fusion with functional lysosomes for the degradation.

The secretion of immature cathepsin B is enhanced in the replicon cell of strain Con1. Lysosomal acidification is required for the cleavage of cathepsins for activation, and cathepsin B (CTSB) is processed under acidic conditions (13). Although a marginal decrease of CTSB was detected in the whole lysates of the SGR^{Con1} cells, a significant reduction in the expression of both unprocessed (pro-CTSB) and matured CTSB was observed in the lysosomal fractions of the SGR^{Con1} cells compared with those of the naïve Huh7 and the SGR^{cured} cells (Fig. 5A). LAMP1 was concentrated at a similar level in

Downloaded from http://jvi.asm.org/ on November 21, 2011 by Yoshiharu Matsuura

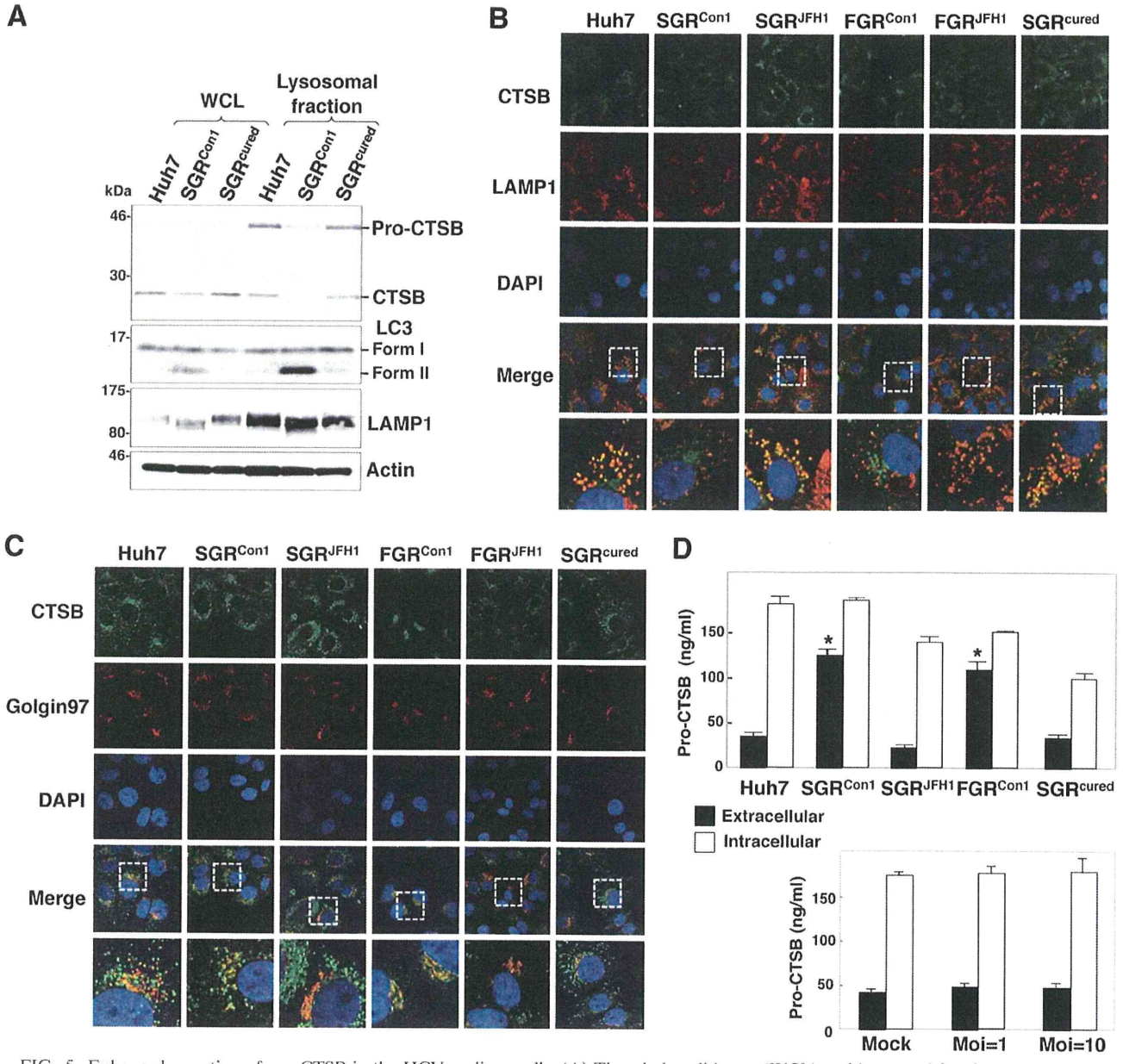

FIG. 5. Enhanced secretion of pro-CTSB in the HCV replicon cells. (A) The whole-cell lysate (WCL) and lysosomal fraction prepared from Huh7, SGR^{Con1}, and SGR^{cured} cells were subjected to immunoblotting. (B and C) Huh7 cells, HCV replicon cells, and SGR^{cured} cells were stained with DAPI, rabbit polyclonal anti-CTSB antibody, and mouse anti-LAMP1 (B) or anti-Golgin97 (C) antibody. The boxed areas in the merged images are magnified. (D) Expression of pro-cathepsin B in the culture supernatants (black bars) and cell lysates (white bars) of the Huh7, SGR^{Con1}, SGR^{JFH1}, FGR^{Con1}, and SGR^{cured} cells and the SGR^{cured} cells infected with HCVcc at a multiplicity of infection (Moi) of 1 or 10 and incubated for 72 h was determined by enzyme-linked immunosorbent assay (ELISA). The error bars indicate standard deviations. The asterisks indicate significant differences ($P < 0.01$) versus the control value. The data shown are representative of three independent experiments.

the lysosomal fractions of the cells, whereas LC-II was detected in the fractions of the SGR^{Con1} cells but not in those of Huh7 and the SGR^{cured} cells, suggesting that autophagosomes and/or autolysosomes in the SGR^{Con1} cells are fractionated in the lysosomal fraction. Colocalization of CTSB with LAMP1 was observed in the naïve Huh7 cells, in the SGR^{cured} cells, and in the replicon cells harboring a sub- or a full genomic RNA of strain JFH1 (SGR^{JFH1} and FGR^{JFH1}, respectively) but not in those of strain Con1 (SGR^{Con1} and FGR^{Con1}) (Fig. 5B). On the other hand, CTSB was colocalized with Golgin97, a marker for the Golgi apparatus, in the SGR^{Con1} and FGR^{Con1} cells but not in other cells (Fig. 5C). Since previous reports suggested that the alkalization in the lysosome triggers secretion of the unprocessed lysosomal enzymes (19, 41), we next determined the secretion of pro-CTSB in the replicon cells. Secretion of the pro-CTSB was significantly enhanced in the replicon cells of strain Con1 but not in those of strain JFH1 and naïve and cured cells (Fig. 5D, top). Furthermore, secretion of pro-CTSB

Downloaded from http://jvi.asm.org/ on November 21, 2011 by Yoshiharu Matsuura

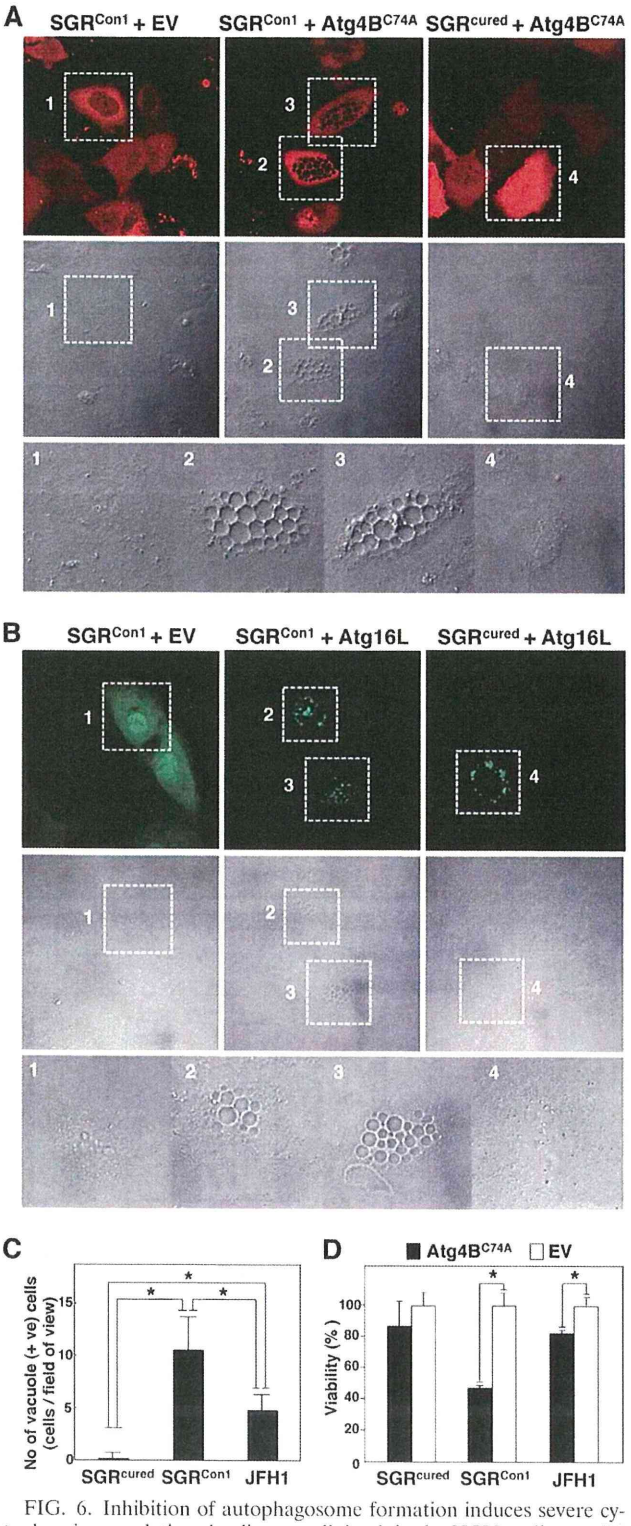

FIG. 6. Inhibition of autophagosome formation induces severe cytoplasmic vacuolations leading to cell death in the HCV replicon cells. (A) SGR^{Con1} and SGR^{cured} cells transfected with pStrawberry-$Atg4B^{C74A}$ or empty vector pStrawberry (EV) were fixed at 48 h posttransfection and examined by fluorescence microscopy. The boxed areas in the phase-contrast images are magnified. (B) SGR^{Con1} and SGR^{cured} cells transfected with pEGFP-Atg16L or EV were examined by fluorescence microscopy at 48 h posttransfection. The boxed areas in the phase-contrast images are magnified. (C) SGR^{cured}, SGR^{Con1}, and SGR^{cured} cells infected with JFH1 virus were transfected with pStrawberry-$Atg4B^{C74A}$, and the number of vacuole-positive cells in each of nine fields of view was counted at 48 h posttransfection. (D) SGR^{cured}, SGR^{Con1}, and SGR^{cured} cells infected with JFH1 virus were transfected with pStrawberry-$Atg4B^{C74A}$ (black bars) or EV (white bars), and cell viability was determined at 6 days posttransfection by using CellTiter-Glo (Promega) according to the manufacturer's protocol. The asterisks indicate significant differences ($P < 0.05$) versus the control value. The data shown are representative of three independent experiments.

was not observed in the cured cells infected with HCVcc, an infectious HCV strain derived from strain JFH1 (Fig. 5D, bottom). Collectively, these results suggest that the dysfunction of lysosomal acidification contributes to the impairment of autophagy in the HCV replicon cells of strain Con1.

Autophagy induced in cells replicating HCV is required for cell survival. Finally, we examined the pathological significance of autophagy during HCV replication. Atg4B is known as an LC3-processing protease, and overexpression of its protease-inactive mutant ($Atg4B^{C74A}$) results in inhibition of the autophagosome formation (7). To our surprise, severe cytoplasmic vacuolation was observed in the SGR^{Con1} cells expressing $Atg4B^{C74A}$ (Fig. 6A). These vacuolations were also observed in the SGR^{Con1} cells by the expression of Atg16L (Fig. 6B), a molecule that is an essential component of the autophagy complex and that, if expressed in excess amounts, can disrupt the autophagosome formation (8). Expression of $Atg4B^{C74A}$ induced a higher level of vacuole formation in the Con1 replicon cells than in cells infected with JFH1 virus but not in the cured cells (Fig. 6C). Along with these vacuolations, cell viability was significantly decreased by the expression of $Atg4B^{C74A}$ in SGR^{Con1} cells and slightly in JFH1 virus-infected cells (Fig. 6D). These results suggest that autophagy induced by the RNA replication of HCV is required for host cell survival.

DISCUSSION

In the present study, we demonstrated that two genotypes of HCV induce autophagy, whereas intact autophagy flux is required for the host cell to survive. The cell death characterized by cytoplasmic vacuolation that was induced in the HCV replicon cells by the inhibition of the autophagosome formation is similar to type III programmed cell death, which is distinguishable from apoptosis and autophagic cell death (4). Type III programmed cell death has been observed in the neurodegenerative diseases caused by the deposit of cytotoxic protein aggregates (15).

We previously reported that HCV hijacks chaperone complexes, which regulates quality control of proteins into the membranous web for circumventing unfolded protein response during efficient genome replication (53); in other words, the replication of HCV exacerbates the generation of proteins associated with cytotoxicity. In the experiments using a chimpanzee model, HCV of genotype 1 was successfully used to reproduce acute and chronic hepatitis similar to that in the human patients (3, 57), and transgenic mice expressing viral proteins of HCV of genotype 1b have been shown to develop

Downloaded from http://jvi.asm.org/ on November 21, 2011 by Yoshiharu Matsuura

Sjögren syndrome, insulin resistance, hepatic steatosis, and hepatocellular carcinoma (27, 28). In contrast, HCVcc, based on the genotype 2a strain JFH1 isolated from a patient with fulminant hepatitis C (33, 56), was unable to establish chronic infection in chimpanzees (56) or to induce cell damage and inflammation in chimeric mice xenotransplanted with human hepatocytes (17). These results imply that the onset of HCV pathogenesis could be dependent not only upon an amount but also on a property of deposited proteins, and they might explain the aggravated vacuolations under the inhibition of autophagosome formation in strain Con1 compared to that in strain JFH1. Interestingly, the overexpression of $Atg4B^{C74A}$ or Atg16L causes eccentric cell death in the Con1 replicon cells in which autophagy flux is already disturbed. Thus, we speculated that the quarantine of undefined abnormalities endowed with high cytotoxicity by the engulfing of the autophagic membrane might be sufficient for the amelioration of HCV-induced degeneration. The autophagosomal dysfunction observed in the Con1 replicon cells may suggest that a replicant of strain Con1 was more sensitive to the lysosomal vacuolation than that of strain JFH1. Because a limitation of our study was that we were unable to use infectious HCV of other strains, it is still unclear whether the autophagic degradation can be impaired only in the replicon of HCV strain Con1 or genotype 1.

We also demonstrated that HCV replication of strain Con1 but not that of strain JFH1 facilitates the secretion of pro-CTSB. It has been well established that the secretion of pro-CTSB is enhanced in several types of tumors (26, 50). The secretion of CTSB, like the secretion of matrix metalloproteases, is a marker of the progression of the proteolytic degradation of the extracellular matrix, which plays an important part in cancer invasion and metastasis. Since infection with HCV of genotype 1 is clinically considered a risk factor for the development of hepatocellular carcinoma (14, 51), the enhanced secretion of pro-CTSB by the replication of genotype 1 strains might synergistically promote infiltration of hepatocellular carcinoma.

As shown elsewhere (see movies in the supplemental material), although most degradations of the autophagosome were impaired due to a dislocalization of a V-ATPase subunit, some autophagic degradation was achieved in the SGR^{Con1} cells similar to that in the starved Huh7 cells. Moreover, the stagnated autophagy flux was rescued by the treatment of alpha interferon accompanied by elimination of HCV (Fig. 1C and D). Interestingly, we observed neither a significant impairment of lysosomal degradation nor the intracellular activity of cathepsins in the replicon cells of HCV strain Con1 (data not shown). Therefore, there might be a specific dysfunction within the autolysosome during the replication of HCV strain Con1. Detailed studies are needed to elucidate how HCV strain Con1 disturbs the sorting of V-ATPase.

A close relationship between autophagy and the immune system has been gradually unveiled (47). Autophagy assists not only in the direct elimination of pathogens by hydrolytic degradation but also in antigen processing in antigen-presenting cells such as macrophage and dendritic cells (DC) for presentation by major histocompatibility complex (MHC) I and II (11). Moreover, autophagy plays important roles in T lymphocyte homeostasis (44). As such, in some instances, interruptions of autophagy can allow microorganisms to escape from the host immune system. Indeed, the immune response against herpes simplex virus was suppressed by blocking the autophagy (6). With regard to HCV, functionally impaired DC dysfunctions marked by poor DC maturation, impaired antigen presentation, and attenuated cytokine production have been reported in tissue culture models and chronic hepatitis C patients (1, 22, 46). In addition, reduction of cell surface expression of MHC-I in HCV genotype 1b replicon cells has been reported (55). We confirmed that levels of cell surface expression of MHC-I in the replicon cells of genotype 1b, but not of genotype 2a, were reduced in comparison with those in the cured cells (data not shown). Hence it might be feasible to speculate that the replication of HCV RNA of genotype 1 induces an incomplete autophagy for attenuating antigen presentation to establish persistent infection. In contrast, autophagy is known to serve as a negative regulator of innate immunity (21, 54). A recent report demonstrated that autophagy induced by infection with strain JFH1 or dengue virus attenuates innate immunity to promote viral replication (23), indicating that an HCV genotype 2a strain may facilitate autophagy to evade innate immunity.

In this study, we demonstrated that HCV utilizes autophagy to circumvent the cell death induced by vacuole formation for its survival. This unique strategy of HCV propagation may provide new clues to the virus-host interaction and, ultimately, to the pathogenesis of infection by various genotypes of HCV.

ACKNOWLEDGMENTS

We thank H. Murase and M. Tomiyama for their secretarial work. We also thank R. Bartenschlager and T. Wakita for providing cell lines and plasmids.

This work was supported in part by grants-in-aid from the Ministry of Health, Labor, and Welfare (Research on Hepatitis), the Ministry of Education, Culture, Sports, Science, and Technology, and the Osaka University Global Center of Excellence Program.

REFERENCES

1. **Auffermann-Gretzinger, S., E. B. Keeffe, and S. Levy.** 2001. Impaired dendritic cell maturation in patients with chronic, but not resolved, hepatitis C virus infection. Blood **97**:3171–3176.
2. **Beyenbach, K. W., and H. Wieczorek.** 2006. The V-type H+ ATPase: molecular structure and function, physiological roles and regulation. J. Exp. Biol. **209**:577–589.
3. **Bradley, D. W.** 2000. Studies of non-A, non-B hepatitis and characterization of the hepatitis C virus in chimpanzees. Curr. Top. Microbiol. Immunol. **242**:1–23.
4. **Clarke, P. G.** 1990. Developmental cell death: morphological diversity and multiple mechanisms. Anat. Embryol. (Berl.) **181**:195–213.
5. **Dreux, M., P. Gastaminza, S. F. Wieland, and F. V. Chisari.** 2009. The autophagy machinery is required to initiate hepatitis C virus replication. Proc. Natl. Acad. Sci. U. S. A. **106**:14046–14051.
6. **English, L., et al.** 2009. Autophagy enhances the presentation of endogenous viral antigens on MHC class I molecules during HSV-1 infection. Nat. Immunol. **10**:480–487.
7. **Fujita, N., et al.** 2008. An Atg4B mutant hampers the lipidation of LC3 paralogues and causes defects in autophagosome closure. Mol. Biol. Cell **19**:4651–4659.
8. **Fujita, N., et al.** 2008. The Atg16L complex specifies the site of LC3 lipidation for membrane biogenesis in autophagy. Mol. Biol. Cell **19**:2092–2100.
9. **Fujitani, Y., C. Ebato, T. Uchida, R. Kawamori, and H. Watada.** 2009. β-cell autophagy: a novel mechanism regulating β-cell function and mass: lessons from β-cell-specific Atg7-deficient mice. Islets **1**:151–153.
10. **Gannage, M., et al.** 2009. Matrix protein 2 of influenza A virus blocks autophagosome fusion with lysosomes. Cell Host Microbe **6**:367–380.
11. **Gannage, M., and C. Munz.** 2009. Autophagy in MHC class II presentation of endogenous antigens. Curr. Top. Microbiol. Immunol. **335**:123–140.
12. **Hara, T., et al.** 2006. Suppression of basal autophagy in neural cells causes neurodegenerative disease in mice. Nature **441**:885–889.
13. **Hasilik, A.** 1992. The early and late processing of lysosomal enzymes: proteolysis and compartmentation. Experientia **48**:130–151.

Downloaded from http://jvi.asm.org/ on November 21, 2011 by Yoshiharu Matsuura

14. **Hatzakis, A., et al.** 1996. Hepatitis C virus 1b is the dominant genotype in HCV-related carcinogenesis: a case-control study. Int. J. Cancer **68:**51–53.
15. **Hirabayashi, M., et al.** 2001. VCP/p97 in abnormal protein aggregates, cytoplasmic vacuoles, and cell death, phenotypes relevant to neurodegeneration. Cell Death Differ. **8:**977–984.
16. **Hiraga, N., et al.** 2011. Rapid emergence of telaprevir resistant hepatitis C virus strain from wildtype clone in vivo. Hepatology (Baltimore, Md.) **54:** 781–788.
17. **Hiraga, N., et al.** 2007. Infection of human hepatocyte chimeric mouse with genetically engineered hepatitis C virus and its susceptibility to interferon. FEBS Lett. **581:**1983–1987.
18. **Ichimura, Y., E. Kominami, K. Tanaka, and M. Komatsu.** 2008. Selective turnover of p62/A170/SQSTM1 by autophagy. Autophagy **4:**1063–1066.
19. **Isidoro, C., et al.** 1995. Altered intracellular processing and enhanced secretion of procathepsin D in a highly deviated rat hepatoma. Int. J. Cancer **60:**61–64.
20. **Jacobson, I. M., P. Cacoub, L. Dal Maso, S. A. Harrison, and Z. M. Younossi.** 2010. Manifestations of chronic hepatitis C virus infection beyond the liver. Clin. Gastroenterol. Hepatol. **8:**1017–1029.
21. **Jounai, N., et al.** 2007. The Atg5 Atg12 conjugate associates with innate antiviral immune responses. Proc. Natl. Acad. Sci. U. S. A. **104:**14050–14055.
22. **Kanto, T., et al.** 1999. Impaired allostimulatory capacity of peripheral blood dendritic cells recovered from hepatitis C virus-infected individuals. J. Immunol. **162:**5584–5591.
23. **Ke, P. Y., and S. S. Chen.** 2011. Activation of the unfolded protein response and autophagy after hepatitis C virus infection suppresses innate antiviral immunity in vitro. J. Clin. Invest. **121:**37–56.
24. **Kimura, S., N. Fujita, T. Noda, and T. Yoshimori.** 2009. Monitoring autophagy in mammalian cultured cells through the dynamics of LC3. Methods Enzymol. **452:**1–12.
25. **Kiyosawa, K., et al.** 1990. Interrelationship of blood transfusion, non-A, non-B hepatitis and hepatocellular carcinoma: analysis by detection of antibody to hepatitis C virus. Hepatology **12:**671–675.
26. **Koblinski, J. E., et al.** 2002. Interaction of human breast fibroblasts with collagen I increases secretion of procathepsin B. J. Biol. Chem. **277:**32220–32227.
27. **Koike, K., et al.** 1997. Sialadenitis histologically resembling Sjogren syndrome in mice transgenic for hepatitis C virus envelope genes. Proc. Natl. Acad. Sci. U. S. A. **94:**233–236.
28. **Koike, K., T. Tsutsumi, H. Yotsuyanagi, and K. Moriya.** 2010. Lipid metabolism and liver disease in hepatitis C viral infection. Oncology **78**(Suppl. 1)**:**24–30.
29. **Komatsu, M., et al.** 2006. Loss of autophagy in the central nervous system causes neurodegeneration in mice. Nature **441:**880–884.
30. **Komatsu, M., et al.** 2007. Homeostatic levels of p62 control cytoplasmic inclusion body formation in autophagy-deficient mice. Cell **131:**1149–1163.
31. **Lee, J. H., et al.** 2010. Lysosomal proteolysis and autophagy require presenilin 1 and are disrupted by Alzheimer-related PS1 mutations. Cell **141:** 1146–1158.
32. **Levine, B., and G. Kroemer.** 2008. Autophagy in the pathogenesis of disease. Cell **132:**27–42.
33. **Lindenbach, B. D., et al.** 2005. Complete replication of hepatitis C virus in cell culture. Science **309:**623–626.
34. **Lohmann, V., et al.** 1999. Replication of subgenomic hepatitis C virus RNAs in a hepatoma cell line. Science **285:**110–113.
35. **Manns, M. P., et al.** 2001. Peginterferon alfa-2b plus ribavirin compared with interferon alfa-2b plus ribavirin for initial treatment of chronic hepatitis C: a randomised trial. Lancet **358:**958–965.
36. **McHutchison, J. G., et al.** 2009. Telaprevir with peginterferon and ribavirin for chronic HCV genotype 1 infection. N. Engl. J. Med. **360:**1827–1838.
37. **Mizushima, N.** 2007. Autophagy: process and function. Genes Dev. **21:**2861–2873.
38. **Moradpour, D., F. Penin, and C. M. Rice.** 2007. Replication of hepatitis C virus. Nat. Rev. Microbiol. **5:**453–463.
39. **Moriishi, K., and Y. Matsuura.** 2007. Host factors involved in the replication of hepatitis C virus. Rev. Med. Virol. **17:**343–354.
40. **Moriishi, K., and Y. Matsuura.** 2003. Mechanisms of hepatitis C virus infection. Antivir. Chem. Chemother. **14:**285–297.
41. **Oda, K., Y. Nishimura, Y. Ikehara, and K. Kato.** 1991. Bafilomycin A1 inhibits the targeting of lysosomal acid hydrolases in cultured hepatocytes. Biochem. Biophys. Res. Commun. **178:**369–377.
42. **Orvedahl, A., et al.** 2007. HSV-1 ICP34.5 confers neurovirulence by targeting the Beclin 1 autophagy protein. Cell Host Microbe **1:**23–35.
43. **Poordad, F., et al.** 2011. Boceprevir for untreated chronic HCV genotype 1 infection. N. Engl. J. Med. **364:**1195–1206.
44. **Pua, H. H., I. Dzhagalov, M. Chuck, N. Mizushima, and Y. W. He.** 2007. A critical role for the autophagy gene Atg5 in T cell survival and proliferation. J. Exp. Med. **204:**25–31.
45. **Ramachandran, N., et al.** 2009. VMA21 deficiency causes an autophagic myopathy by compromising V-ATPase activity and lysosomal acidification. Cell **137:**235–246.
46. **Saito, K., et al.** 2008. Hepatitis C virus inhibits cell surface expression of HLA-DR, prevents dendritic cell maturation, and induces interleukin-10 production. J. Virol. **82:**3320–3328.
47. **Schmid, D., and C. Munz.** 2007. Innate and adaptive immunity through autophagy. Immunity **27:**11–21.
48. **Schutte, K., J. Bornschein, and P. Malfertheiner.** 2009. Hepatocellular carcinoma—epidemiological trends and risk factors. Dig. Dis. **27:**80–92.
49. **Sir, D., et al.** 2008. Induction of incomplete autophagic response by hepatitis C virus via the unfolded protein response. Hepatology **48:**1054–1061.
50. **Sloane, B. F., et al.** 2005. Cathepsin B and tumor proteolysis: contribution of the tumor microenvironment. Semin. Cancer Biol. **15:**149–157.
51. **Stankovic-Djordjevic, D., et al.** 2007. Hepatitis C virus genotypes and the development of hepatocellular carcinoma. J. Dig. Dis. **8:**42–47.
52. **Strader, D. B., T. Wright, D. L. Thomas, and L. B. Seeff.** 2004. Diagnosis, management, and treatment of hepatitis C. Hepatology **39:**1147–1171.
53. **Taguwa, S., et al.** 2009. Cochaperone activity of human butyrate-induced transcript 1 facilitates hepatitis C virus replication through an Hsp90-dependent pathway. J. Virol. **83:**10427–10436.
54. **Tal, M. C., et al.** 2009. Absence of autophagy results in reactive oxygen species-dependent amplification of RLR signaling. Proc. Natl. Acad. Sci. U. S. A. **106:**2770–2775.
55. **Tardif, K. D., and A. Siddiqui.** 2003. Cell surface expression of major histocompatibility complex class I molecules is reduced in hepatitis C virus subgenomic replicon-expressing cells. J. Virol. **77:**11644–11650.
56. **Wakita, T., et al.** 2005. Production of infectious hepatitis C virus in tissue culture from a cloned viral genome. Nat. Med. **11:**791–796.
57. **Walker, C. M.** 1997. Comparative features of hepatitis C virus infection in humans and chimpanzees. Springer Semin. Immunopathol. **19:**85–98.
58. **Wasley, A., and M. J. Alter.** 2000. Epidemiology of hepatitis C: geographic differences and temporal trends. Semin. Liver Dis. **20:**1–16.
59. **Wong, J., et al.** 2008. Autophagosome supports coxsackievirus B3 replication in host cells. J. Virol. **82:**9143–9153.
60. **Yoshimori, T., and T. Noda.** 2008. Toward unraveling membrane biogenesis in mammalian autophagy. Curr. Opin. Cell Biol. **20:**401–407.

Downloaded from http://jvi.asm.org/ on November 21, 2011 by Yoshiharu Matsuura

JOURNAL OF VIROLOGY, Nov. 2011, p. 10976–10988 Vol. 85, No. 21
0022-538X/11/$12.00 doi:10.1128/JVI.00846-11
Copyright © 2011, American Society for Microbiology. All Rights Reserved.

Heterogeneous Nuclear Ribonucleoprotein A2 Participates in the Replication of Japanese Encephalitis Virus through an Interaction with Viral Proteins and RNA▽

Hiroshi Katoh,[1] Yoshio Mori,[3] Hiroto Kambara,[1] Takayuki Abe,[1] Takasuke Fukuhara,[1] Eiji Morita,[1] Kohji Moriishi,[4] Wataru Kamitani,[2] and Yoshiharu Matsuura[1]*

Department of Molecular Virology[1] and Global COE Program,[2] Research Institute for Microbial Diseases, Osaka University, Osaka, Department of Virology III, National Institute of Infectious Diseases, Tokyo,[3] and Department of Microbiology, Faculty of Medicine, Yamanashi University, Yamanashi,[4] Japan

Received 26 April 2011/Accepted 9 August 2011

Japanese encephalitis virus (JEV) is a mosquito-borne flavivirus that is kept in a zoonotic transmission cycle between pigs and mosquitoes. JEV causes infection of the central nervous system with a high mortality rate in dead-end hosts, including humans. Many studies have suggested that the flavivirus core protein is not only a component of nucleocapsids but also an important pathogenic determinant. In this study, we identified heterogeneous nuclear ribonucleoprotein A2 (hnRNP A2) as a binding partner of the JEV core protein by pulldown purification and mass spectrometry. Reciprocal coimmunoprecipitation analyses in transfected and infected cells confirmed a specific interaction between the JEV core protein and hnRNP A2. Expression of the JEV core protein induced cytoplasmic retention of hnRNP A2 in JEV subgenomic replicon cells. Small interfering RNA (siRNA)-mediated knockdown of hnRNP A2 resulted in a 90% reduction of viral RNA replication in cells infected with JEV, and the reduction was cancelled by the expression of an siRNA-resistant hnRNP A2 mutant. In addition to the core protein, hnRNP A2 also associated with JEV nonstructural protein 5, which has both methyltransferase and RNA-dependent RNA polymerase activities, and with the 5′-untranslated region of the negative-sense JEV RNA. During one-step growth, synthesis of both positive- and negative-strand JEV RNAs was delayed by the knockdown of hnRNP A2. These results suggest that hnRNP A2 plays an important role in the replication of JEV RNA through the interaction with viral proteins and RNA.

Japanese encephalitis virus (JEV) belongs to the genus *Flavivirus* within the family *Flaviviridae*. Members of the genus *Flavivirus* are predominantly arthropod-borne viruses, such as dengue virus (DEN), West Nile virus (WNV), yellow fever virus (YFV), and tick-borne encephalitis virus, and frequently cause significant morbidity and mortality in mammals and birds (46). JEV is distributed in the south and southeast regions of Asia and is kept in a zoonotic transmission cycle between pigs or birds and mosquitoes (46, 69). JEV spreads to dead-end hosts, including humans, through the bite of JEV-infected mosquitoes and causes infection of the central nervous system, with a high mortality rate (46). JEV has a single-stranded positive-strand RNA genome of approximately 11 kb, which is capped at the 5′ end but lacks modification of the 3′ terminus by polyadenylation (38). The genomic RNA carries a single large open reading frame, and a polyprotein translated from the genome is cleaved co- and posttranslationally by host and viral proteases to yield three structural proteins—the core, precursor membrane, and envelope protein—and seven nonstructural (NS) proteins—NS1, NS2A, NS2B, NS3, NS4A, NS4B, and NS5 (61).

The core protein of flaviviruses has RNA-binding activity through basic amino acid clusters located in both the amino and carboxyl termini, indicating that the core protein forms a nucleocapsid interacting with viral RNA (23). In spite of the replication of flaviviruses in the cytoplasm, the core protein is also detected in the nucleus, especially the nucleolus, suggesting that the core protein plays an additional role in the life cycle of flaviviruses (6, 42, 48, 66). We previously reported that a mutant JEV defective in the nuclear localization of the core protein had impaired growth in mammalian cells and impaired neuroinvasiveness in mice (48) and that the nuclear and cytoplasmic localization of the JEV core protein is dependent on binding to the host nucleolar protein B23 (62). In addition to the JEV core protein, other flavivirus core proteins bind to several host proteins, such as Jab (a component of the COP9 signalosome complex) (53), the chaperone protein Hsp70 (54), heterogeneous nuclear ribonucleoprotein (hnRNP) K (7), and the apoptotic proteins HDM2 (71) and Daxx (50), and regulate their functions. In the cytoplasm, the core protein of flaviviruses was found at the sites of viral RNA replication (40, 68). A recent report demonstrated a coupling between viral RNA synthesis and RNA encapsidation (21, 55, 61). Therefore, the flavivirus core protein plays crucial roles not only in the viral life cycle, including RNA replication and assembly, but also in viral pathogenesis.

Replication of flaviviruses is initiated by a viral RNA replication complex through a process of RNA-dependent RNA polymerization on the endoplasmic reticulum (ER) membranes. The intracellular membrane rearrangements that are induced by the *Flaviviridae* family are best characterized for Kunjin virus (KUN), which is the Australian variant of WNV

* Corresponding author. Mailing address: Department of Molecular Virology, Research Institute for Microbial Diseases, Osaka University, 3-1 Yamada-oka, Suita, Osaka 565-0871, Japan. Phone: 81-6-6879-8340. Fax: 81-6-6879-8269. E-mail: matsuura@biken.osaka-u.ac.jp.

▽ Published ahead of print on 24 August 2011.

Downloaded from http://jvi.asm.org/ on November 21, 2011 by Yoshiharu Matsuura

(14). KUN induces two distinct membrane structures: large clusters of double-membrane vesicles (DMV) and a second membrane structure that consists of convoluted membranes (CM). It has been demonstrated that DMV are the sites of viral replication, whereas CM are the sites of viral polyprotein processing (67). Clusters of DMV have also been observed in other flaviviruses (65). The NS3 and NS5 proteins have been identified as the major components of the viral RNA replication complex (4). NS5, the largest and most conserved flavivirus protein, contains sequences homologous to those of methyltransferase (MTase) and RNA-dependent RNA polymerase (RdRp), which are responsible for methylation of the 5′ cap structure (9, 27) and for viral RNA replication (1, 12, 74), respectively. In addition, NS5 inhibits the interferon-stimulated Jak-Stat signaling pathway through the activation of protein tyrosine phosphatases during JEV infection (37).

In this study, we identified hnRNP A2 as a binding partner of the JEV core protein by pulldown purification and mass spectrometry. hnRNP A2 and B1, which are the most abundant of the approximately 20 major hnRNPs, are produced by alternative splicing from a single gene and differ from each other by only a 12-amino-acid insertion in the N-terminal region of A2 (28). hnRNP A2 participates in posttranscriptional regulation in both the nucleus and cytoplasm and also is involved in telomere biogenesis. hnRNP A2 was translocated from the nucleus to the cytoplasm upon infection with JEV and facilitated viral replication through interaction with the JEV core and NS5 proteins and with the 5′-untranslated region (UTR) of the negative-strand JEV RNA, suggesting an important role for hnRNP A2 in the life cycle of JEV.

MATERIALS AND METHODS

Cells. Vero (African green monkey kidney), 293T (human kidney), and Huh7 (human hepatocellular carcinoma) cells were maintained in Dulbecco's modified Eagle's minimal essential medium (DMEM) supplemented with 100 U/ml penicillin, 100 μg/ml streptomycin, nonessential amino acids (Sigma, St. Louis, MO), and 10% fetal bovine serum (FBS). JEV subgenomic replicon (SGR) cells were generated as described previously (18). Briefly, Huh7 and 293T cells were electroporated with *in vitro*-transcribed RNA from pJErepIRESpuro, and drug-resistant clones were selected by treatment with puromycin (Invivogen, San Diego, CA) at a final concentration of 1 μg/ml. The resulting replicon cells were designated JEV-SGR-Huh7 and JEV-SGR-293T cells, respectively. Cell viability was determined by using CellTiter-Glo (Promega, Madison, WI) according to the manufacturer's instructions.

Plasmids. Plasmids encoding hemagglutinin (HA)-, FLAG-, and MEF (consisting of a myc tag, the tobacco etch virus protease cleavage site, and a FLAG tag)-tagged JEV core (pCAGPM-Core-HA, pCAGPM-FLAG-Core, and pCAGPM-MEF-Core, respectively) were prepared as described previously (49, 62). Plasmids encoding HA-tagged JEV NS proteins (pCAGPM-HA-NS) were generated by previously described methods (18). The cDNA of human hnRNP A2 was amplified by PCR and cloned into pcDNA 3.1 containing a FLAG tag gene (pcDNA 3.1 N-FLAG) (62), pCAGPM containing an HA tag gene (pCAGPM N-HA) (48), and pGEX 4T-1 (GE Healthcare, Buckinghamshire, United Kingdom) for expression in bacteria as a glutathione *S*-transferase (GST) fusion protein. The resulting plasmids were designated pcDNA-FLAG-hnRNP A2, pCAGPM-HA-hnRNP A2, and pGEX-hnRNP A2, respectively. A series of deletion mutants of the core protein, NS5, and hnRNP A2 was synthesized by PCR-based mutagenesis using a KOD-Plus mutagenesis kit (Toyobo, Osaka, Japan). A silent mutant of HA-hnRNP A2 (siR) and a mutant of FLAG-tagged core with Gly^{42} and Pro^{43} replaced by Ala (FLAG-CoreM) were also generated by PCR-based mutagenesis. All plasmids were confirmed by sequencing with an ABI Prism 3130 genetic analyzer (Applied Biosystems, Tokyo, Japan).

Antibodies. Anti-JEV core rabbit polyclonal antibody (PAb) was prepared as described previously (48). Anti-JEV NS3 mouse monoclonal antibody (MAb) was prepared by using a recombinant protein spanning amino acids (aa) 171 to 619 of JEV NS3. Anti-JEV NS5 mouse MAb was generated with recombinant NS5 at Bio Matrix Research Inc. (Chiba, Japan). Anti-FLAG mouse MAb (M2), anti-hnRNP A2/B1 mouse MAb (DP3B3), anti-β-actin mouse MAb, and anti-FLAG rabbit PAb were purchased from Sigma. Anti-nucleoporin p62 mouse MAb and anti-GM130 mouse MAb were purchased from BD Biosciences (Franklin Lakes, NJ). Anti-JEV envelope protein mouse MAb (6B4A-10), anti-HA mouse MAb (HA11), anti-PA28α rabbit PAb, anti-calregulin rabbit PAb (H-170), and anti-HA rat MAb (3F10) were purchased from Chemicon (Temecula, CA), Covance (Richmond, CA), Affinity Bioreagents (Golden, CO), Santa Cruz (California, CA), and Roche (Mannheim, Germany), respectively.

MEF purification. pCAGPM-MEF-Core was transfected into 293T cells and subjected to MEF purification as described previously (17, 62). Proteins interacting with the JEV core protein were separated by 12.5% sodium dodecyl sulfate-polyacrylamide gel electrophoresis (SDS-PAGE) and visualized by silver staining. The stained bands were excised, digested in gels with Lys-C, and analyzed by direct nanoflow liquid chromatography-tandem mass spectrometry (LC-MS/MS) (17).

Transfection, immunoprecipitation, and immunoblotting. Plasmids were transfected into 293T cells by use of TransIT LT1 (Mirus, Madison, WI), and cells were harvested at 24 h posttransfection and subjected to immunoprecipitation and immunoblotting as described previously (15). The immunoprecipitates were boiled in loading buffer and subjected to 12.5% or 15% SDS-PAGE. The proteins were transferred to polyvinylidene difluoride membranes (Millipore, Bedford, MA) and incubated with the appropriate antibodies. The immune complexes were visualized with SuperSignal West Femto substrate (Thermo Scientific, Rockford, IL) and detected by use of an LAS-3000 image analyzer system (Fujifilm, Tokyo, Japan).

Immunofluorescence microscopy and subcellular fractionation. Vero cells infected with JEV at a multiplicity of infection (MOI) of 1.0 or JEV-SGR-Huh7 cells transfected with pCAGPM-FLAG-Core and/or pCAGPM-HA-hnRNP A2 were fixed with cold acetone, incubated with appropriate antibodies, and examined by use of a Fluoview FV1000 laser scanning confocal microscope (Olympus, Tokyo, Japan) at 24 h postinfection/posttransfection. The subcellular localization of the proteins was determined by fractionation using a nuclear/cytosol fractionation kit (Biovision, Mountain, CA) according to the manufacturer's instructions.

Gene silencing. The small interfering RNAs (siRNAs) si-A2#1 (5′-GGAUU AUUUAAUAACAUU-3′) and si-A2#2 (5′-GGAGAGUAGUUGAGCCAA A-3′) (47) were used for knockdown of endogenous hnRNA A2/B1. The negative control, siCONTROL nontargeting siRNA-2 (si-NC), which exhibits no downregulation of any human genes, was purchased from Dharmacon (Buckinghamshire, United Kingdom). JEV-SGR-293T and naïve 293T cells grown on 6-, 12-, and 24-well plates were transfected with 30, 12, and 6 nM siRNA, respectively, by use of Lipofectamine RNAiMax (Invitrogen, Carlsbad, CA).

Real-time PCR. Total RNA was prepared from cells by use of an RNeasy minikit (Qiagen, Tokyo, Japan), and first-strand cDNA was synthesized using a ReverTra Ace qPCR RT kit (Toyobo). The level of each cDNA was determined by using Platinum SYBR green qPCR SuperMix UDG (Invitrogen), and fluorescent signals were analyzed by use of an ABI Prism 7000 system (Applied Biosystems). Strand-specific reverse transcription (RT) was performed using the following primers: 5′-ATGAGGCTGCCACACCAGAT-3′ for positive-strand JEV RNA, 5′-TACTCCGACGGTGTGGTCTA-3′ for negative-strand JEV RNA, and an oligo(dT) primer for β-actin mRNA. The JEV NS5 and β-actin genes were amplified using the following primer pairs: 5′-GCCGGGTGGGAC ACTAGAAT-3′ and 5′-TGGACAGCGATGTTCGTGAA-5′ for NS5 and 5′-A CGGGGTCACCCACACTGTGC-3′ and 5′-CTAGAAGCATTTGCGGTGGA CGATG-3′ for β-actin. The value of JEV RNA was normalized to that of β-actin mRNA.

Virus titration. Virus infectivity was determined by an immunostaining focus assay with Vero cells and was expressed in focus-forming units (FFU). Briefly, viruses were serially diluted and inoculated onto monolayers of Vero cells. After 1 h of absorption, cells were washed with serum-free DMEM and cultured in DMEM containing 5% FBS and 1.25% methylcellulose 4000. At 48 h postinfection, cells were fixed with 4% paraformaldehyde and permeabilized with 0.5% Triton X-100, and infectious foci were stained with anti-JEV envelope protein mouse MAb (6B4A-10) and visualized with a Vectastain Elite ABC anti-mouse IgG kit with VIP substrate (Vector Laboratories, Burlingame, CA).

Immunoprecipitation–RT-PCR. Cells (1×10^6) transfected with pCAGPM-HA-hnRNP A2 were infected with JEV at an MOI of 1.0 and then incubated with 400 μl of RNA-protein binding buffer (10 mM HEPES [pH 7.3], 500 mM KCl, 1 mM EDTA, 2 mM $MgCl_2$, 0.1% NP-40, yeast tRNA [0.1 μg/μl], RNase inhibitor [1 U/ml] [Toyobo], and protease inhibitor cocktail [Complete; Roche]) for 10 min at 4°C at 24 h postinfection. After centrifugation at 16,000 × *g* at 4°C for 20 min, the supernatants were incubated with 20 μl of protein G-Sepharose

Downloaded from http://jvi.asm.org/ on November 21, 2011 by Yoshiharu Matsuura

4B Fast Flow beads (GE Healthcare) and 1 μg of normal mouse IgG for 1 h at 4°C. After centrifugation, the supernatants were further incubated with 1 μg of anti-HA mouse MAb or normal mouse IgG for 2 h at 4°C, and 25 μl of protein G-Sepharose beads was added. After 1 h of incubation at 4°C, the beads were washed five times with RNA-protein binding buffer without yeast tRNA, and RNA was isolated by use of TRIzol reagent (Invitrogen). RT-PCR was carried out using random hexamers and PrimeScript II reverse transcriptase (Takara Bio, Shiga, Japan), followed by PCR with PrimeSTAR GXL DNA polymerase (Takara Bio) and primers (5′-TCTGTCACTAGACTGGAGCA-3′ and 5′-CCA GAAACATCACCAGAAGG-3′) targeted to a fragment consisting of nucleotides 2652 to 3589 in the JEV NS1 gene.

***In vitro* transcription.** cDNA fragments encoding either the positive or negative strand of the 5′ and 3′ UTRs of JEV under the control of the T7 promoter were amplified by PCR. RNA transcripts were synthesized using a MEGAscript T7 kit (Ambion, Austin, TX). Biotinylated RNA was synthesized by adding 20 pmol of biotinylated UTP (biotin-16-UTP; Roche) to a 20-μl MEGAscript transcription reaction mix. Synthesized RNAs were purified using phenol-chloroform extraction and isopropanol precipitation and were analyzed in a 2% agarose gel.

RNA pulldown assay. Cell lysates (200 μg) extracted from 293T cells expressing HA-hnRNP A2 were incubated for 15 min at 30°C with the biotinylated JEV UTR RNA (10 pmol) in RNA-protein binding buffer and further incubated for 10 min at room temperature after addition of 250 μl streptavidin-conjugated MagneSphere paramagnetic particles (Promega). The RNA-protein complexes were washed five times with RNA-protein binding buffer without yeast tRNA and then subjected to SDS-PAGE and immunoblotting after boiling in 25 μl 2× SDS-PAGE sample buffer.

Preparation of recombinant hnRNP A2 and GST pulldown assay. GST-fused hnRNP A2 was expressed in *Escherichia coli* BL21(DE3) cells transformed with pGEX-hnRNP A2. Bacteria grown to an optical density at 600 nm of 0.6 were induced with 0.1 mM isopropyl-β-D-thiogalactopyranoside, incubated for 4 h at 37°C with shaking, collected by centrifugation at 6,000 × *g* for 10 min, lysed in 10 ml lysis buffer (50 mM Tris-HCl, pH 7.4, 150 mM NaCl, 1 mM EDTA, 1% Triton X-100) by sonication on ice, and centrifuged at 10,000 × *g* for 20 min. The supernatant was mixed with 200 μl of glutathione-Sepharose 4B beads (GE Healthcare) equilibrated with lysis buffer for 1 h at room temperature, and the beads were washed five times with lysis buffer and then replaced with RNA-protein binding buffer. Ten micrograms of GST or GST-hnRNP A2 was mixed with 10 pmol of the biotinylated positive or negative strand of the 3′ or 5′ UTR of JEV RNA for 15 min at 30°C with gentle agitation. The beads were washed five times with RNA-protein binding buffer without yeast tRNA.

Northern blotting. RNAs interacting with proteins were isolated by use of TRIzol reagent, separated by use of a formaldehyde-free RNA gel electrophoresis system (Amresco, Solon, OH), and transferred to a positively charged nylon membrane (Roche). The biotinylated RNA was detected with streptavidin conjugated with alkaline phosphatase (Roche) and visualized by chemiluminescence using CSPD (Roche).

RESULTS

Identification of hnRNP A2 as a binding partner of the JEV core protein. To identify cellular proteins associated with the JEV core protein, we employed an MEF affinity tag purification method. The MEF-Core protein was expressed in 293T cells and purified together with associated proteins as described previously (62). The silver-stained proteins were excised from an SDS-PAGE gel and analyzed by use of a nanoflow LC-MS/MS system. This procedure identified the amino acid sequences QEMQEVQSSR and GGGGNFGPGPGS NFR, which respond to amino acid residues 179 to 188 and 202 to 206 of human hnRNP A2, respectively. To confirm the interaction between the JEV core protein and hnRNP A2 in cells, 293T cells expressing FLAG-Core and HA-hnRNP A2 were examined by immunoprecipitation analyses. FLAG-Core and HA-hnRNP A2 were shown to be immunoprecipitated with each other (Fig. 1A). Furthermore, endogenous hnRNP A2 was coprecipitated with the JEV core protein in 293T cells infected with JEV but not in mock-infected cells (Fig. 1B). These results indicate that hnRNP A2 interacts with the JEV core protein.

Next, to determine the regions responsible for the interaction between JEV core and hnRNP A2, series of deletion mutants of the JEV core protein and hnRNP A2 were generated and examined by immunoprecipitation analyses. FLAG-Core (full length) and mutants lacking the N-terminal 20 and 40 amino acid residues (ΔN20 and ΔN40), but not those lacking the C-terminal 20 and 40 amino acid residues (ΔC65 and ΔC85), were immunoprecipitated with HA-hnRNP A2 (Fig. 1C). The flavivirus core protein has been shown to form homodimers via the central and C-terminal regions (26, 39). Therefore, to exclude the possibility that C-terminal deletion of the core protein abrogates dimerization, FLAG-Core (full length or ΔC85) and Core-HA (full length or ΔC85) were coexpressed and immunoprecipitated. As shown in Fig. 1D, the C-terminal deletion exhibited no effect on the homotypic interaction of the core protein, consistent with previous data showing that deletion of the C-terminal amino acid residues (aa 73 to 100) did not abolish the homotypic interaction of DEN core protein (64). These results indicate that the C-terminal region (aa 85 to 104) of the JEV core protein is responsible for the protein-protein interaction with hnRNP A2. hnRNP A2 is composed of two N-terminal RNA recognition motifs (RRM) followed by a Gly-rich C-terminal domain (GRD) (29). FLAG-hnRNP A2 (full length) and a mutant lacking the RRM1 domain (ΔRRM1), but not mutants lacking either RRM2 (ΔRRM2) or GRD (ΔGRD), were immunoprecipitated with Core-HA (Fig. 1E). The results indicated that the C-terminal residues from positions 85 to 104 of the JEV core protein and RRM2 and GRD in hnRNP A2 are responsible for the interaction.

hnRNP A2 translocates from the nucleus to the cytoplasm upon infection with JEV. To examine the intracellular localization of hnRNP A2 in cells infected with JEV, Vero cells expressing HA-hnRNP A2 were infected with JEV because an anti-hnRNP A2 antibody capable of detecting endogenous hnRNP A2 by immunofluorescence analysis was not available. We employed Vero cells, which exhibit a wider cytoplasm space than 293T cells, to investigate the cellular localization of each protein. Although HA-hnRNP A2 was detected mainly in the nucleus in mock-infected cells, as previously described (19), translocation of HA-hnRNP A2 into the nucleolus and cytoplasm and colocalization with the core protein were observed upon infection with JEV (Fig. 2A). HA-hnRNP A2 was detected in both the nucleus and cytoplasm in <60% of cells infected with JEV, while only 5% of mock-infected cells exhibited cytoplasmic localization of HA-hnRNP A2 (Fig. 2B). To further confirm the subcellular localization of hnRNP A2, the cytoplasmic and nuclear fractions of JEV-infected cells were analyzed by immunoblotting (Fig. 2C). hnRNP A2 was detected in both the cytoplasmic and nuclear fractions of the JEV-infected cells, while it was detected mainly in the nuclei of the mock-infected cells. These results indicate that infection of JEV induces translocation of hnRNP A2 from the nucleus to the cytoplasm.

Knockdown of hnRNP A2 decreases propagation of JEV. To determine the role of hnRNP A2 in the propagation of JEV, JEV was inoculated into 293T cells transfected with two siRNAs targeted to hnRNP A2/B1 (si-A2#1 and -2) or with a

Downloaded from http://jvi.asm.org/ on November 21, 2011 by Yoshiharu Matsuura

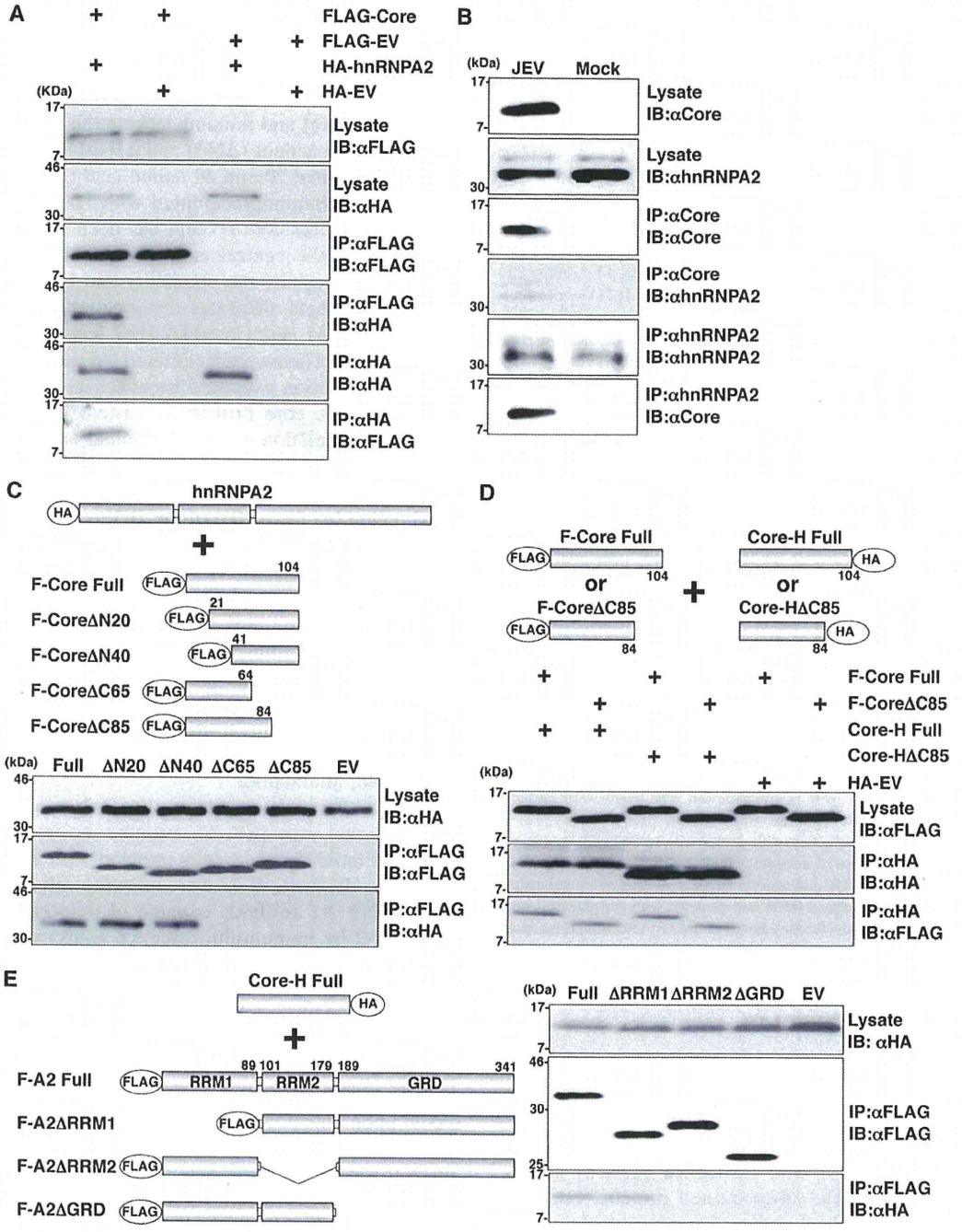

FIG. 1. Interaction of JEV core protein with hnRNP A2. (A) FLAG-Core and HA-hnRNP A2 were coexpressed in 293T cells and immunoprecipitated (IP) with mouse anti-HA MAb (HA11) or mouse anti-FLAG MAb (M2). The immunoprecipitates were subjected to immunoblotting (IB) to detect coprecipitated counterparts. As a negative control, an empty vector (EV) was used. (B) Interaction of JEV core protein with endogenous hnRNP A2 in 293T cells infected with JEV. Cells infected with JEV at an MOI of 1.0 were lysed at 24 h postinfection, and JEV core protein or hnRNP A2 was immunoprecipitated with rabbit anti-core PAb or mouse anti-hnRNP A2 MAb (DP3B3). The precipitates were analyzed by IB with appropriate antibodies. (C) Interaction of hnRNP A2 with deletion mutants of the JEV core protein. HA-hnRNP A2 and a series of deletion mutants of FLAG-Core were cotransfected in 293T cells, precipitated with mouse anti-FLAG MAb (M2), and then subjected to IB. (D) Dimerization of C-terminal deletion mutants of JEV core protein. FLAG-Core (full or ΔC85) and Core-HA (full or ΔC85) were cotransfected into 293T cells, treated with RNase A (10 μg/ml) for 30 min at 4°C, precipitated with mouse anti-HA MAb (HA11), and then subjected to IB. (E) Interaction of JEV core protein with deletion mutants of hnRNP A2. Core-HA and a series of deletion mutants of FLAG-hnRNP A2 were cotransfected into 293T cells and processed as described for panel C.

Downloaded from http://jvi.asm.org/ on November 21, 2011 by Yoshiharu Matsuura

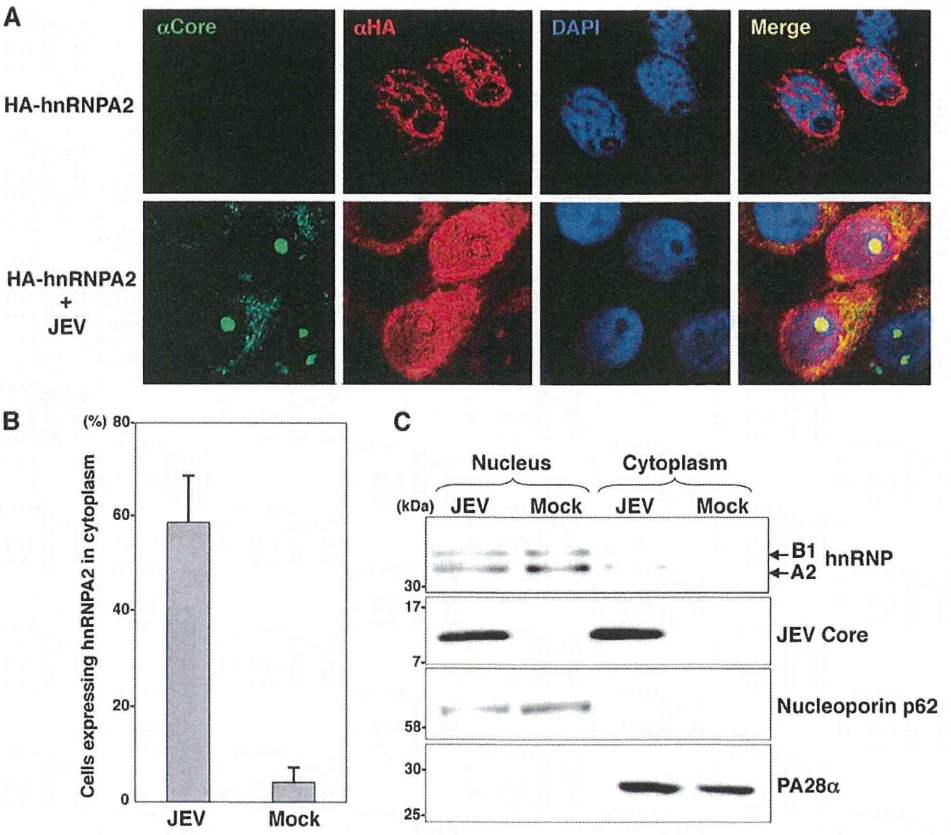

FIG. 2. Translocation of hnRNP A2 from the nucleus to the cytoplasm upon infection with JEV. (A) Vero cells transfected with a plasmid encoding HA-hnRNP A2 were infected with JEV at an MOI of 1.0 and then fixed with cold acetone at 24 h postinfection. JEV core and HA-hnRNP A2 were stained with rabbit anti-core PAb and mouse anti-HA MAb (HA11), followed by AF488-conjugated anti-rabbit IgG and AF594-conjugated anti-mouse IgG antibodies, respectively. Cell nuclei were stained with DAPI (4′,6-diamidino-2-phenylindole) (blue). (B) Percentages of cells exhibiting translocation of HA-hnRNP A2 to the cytoplasm. Three hundred cells expressing HA-hnRNP A2 were counted in three independent experiments. Error bars indicate the standard deviations of the means. (C) Intracellular fractionation of 293T cells infected with JEV. JEV core and hnRNP A2 in the nuclear and cytoplasmic fractions were detected by immunoblotting with rabbit anti-core PAb and mouse anti-hnRNP A2 MAb (DP3B3), respectively. Nucleoporin p62 and PA28α were used as nuclear and cytoplasmic markers, respectively.

control siRNA (si-NC) at 24 h posttransfection. Transfection of the siRNAs exhibited no cytotoxicity, so total RNA was extracted from the infected cells, and the level of JEV RNA was determined by real-time PCR at 24 h postinfection (Fig. 3A). The levels of JEV RNAs in cells transfected with si-A2#1 and -2 were reduced by approximately 40% and 90%, respectively, compared with those in cells treated with si-NC. The expression of JEV NS3 protein was decreased in accord with the reduction of hnRNP A2 (Fig. 3B). Furthermore, a reduction of viral production in the culture supernatants was observed by the knockdown of hnRNP A2 (Fig. 3C). To confirm the specificity of the suppression of JEV propagation by the knockdown of hnRNP A2, a mutant HA-hnRNP A2 protein resistant to si-A2#2 by the introduction of silent mutations (siR) was introduced into cells transfected with si-A2#2 (Fig. 3D). The reduction of JEV RNA propagation by the knockdown of hnRNP A2 was partially rescued by the expression of siR. These results suggest that hnRNP A2 is required for the propagation of JEV.

Translocation of hnRNP A2 from the nucleus to the ER by expression of JEV core protein enhances viral replication. Next, to determine the biological significance of hnRNP A2 in the replication of JEV RNA, we examined the effect of knockdown of hnRNP A2 in JEV-SGR-293T cells, since the subgenomic replicon RNA of JEV replicates autonomously in 293T cells in the absence of structural proteins. Knockdown of hnRNP A2 in the JEV-SGR-293T cells had no significant effect on the replication of the subgenomic RNA and the expression of the NS3 protein (Fig. 4A), suggesting that hnRNP A2 requires JEV structural proteins, probably the core protein, to enhance viral replication. To assess this possibility, we examined the effect of the exogenous expression of the JEV core protein on the subcellular localization of hnRNP A2 and the replication of the subgenomic RNA. HA-hnRNP A2 and FLAG-Core were coexpressed in subgenomic replicon Huh7 cells (JEV-SGR-Huh7) because these replicon cells were established in our laboratory previously (18). Huh7 cells exhibit a wider cytoplasmic view than 293T cells but have smaller and fewer nucleoli than Vero cells. HA-hnRNP A2 was detected in the nuclei of the Huh7 replicon cells transfected with an empty plasmid (Fig. 4B). Although FLAG-Core was not colocalized with calregulin, GM130, and EEA1, which are markers of the ER, Golgi apparatus, and early endosome, respectively, HA-hnRNP A2 was colocalized with FLAG-Core

Downloaded from http://jvi.asm.org/ on November 21, 2011 by Yoshiharu Matsuura

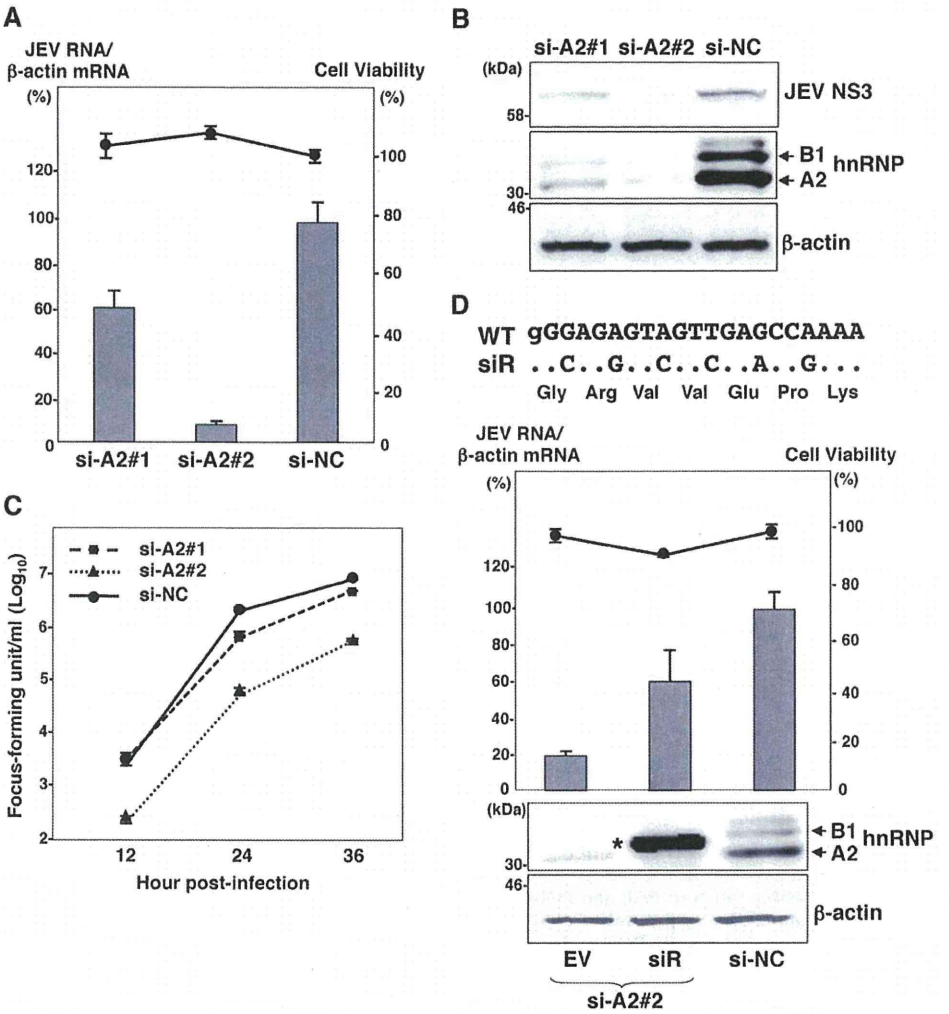

FIG. 3. Effect of hnRNP A2 knockdown on JEV propagation. (A) JEV was infected with 293T cells at an MOI of 1.0 24 h after transfection with si-A2#1, si-A2#2, or si-NC. Total cellular RNA was extracted at 24 h postinfection and subjected to RT. The level of JEV RNA (NS5) was determined by real-time PCR and calculated as a percentage of the control β-actin mRNA level (bar graph). Cell viability was determined 48 h after transfection with each siRNA and calculated as a percentage of the viability of cells treated with si-NC (line graph). The data are representative of three independent experiments. Error bars indicate the standard deviations of the means. (B) Cell lysates collected at 24 h postinfection were subjected to immunoblotting with mouse MAbs to JEV NS3, hnRNP A2 (DP3B3), and β-actin. (C) Culture supernatants were harvested at 12, 24, and 36 h postinfection, and infectious titers were determined by focus-forming assays in Vero cells. Closed squares, triangles, and circles indicate the infectious titers in the culture supernatants of cells transfected with si-A2#1, si-A2#2, and si-NC, respectively. The results shown are from three independent assays, with the error bars representing the standard deviations. (D) (Top) Nucleotide and amino acid sequences of wild-type (WT) and siRNA-resistant (siR) HA-hnRNP A2. Capital letters in the WT sequence indicate the target sequence of si-A2#2, and dots indicate the same nucleotides. (Middle) 293T cells cotransfected with si-A2#2 and siR or empty vector (EV) or transfected with si-NC were infected with JEV at an MOI of 1.0 at 24 h posttransfection. Total cellular RNA was extracted at 24 h postinfection and subjected to RT. The level of JEV RNA (NS5) was determined by real-time PCR and calculated as a percentage of the control β-actin mRNA level (bar graph). Cell viability was determined 48 h after transfection with each siRNA and calculated as a percentage of the viability of cells treated with si-NC (line graph). (Bottom) Cell lysates collected at 24 h postinfection were subjected to immunoblotting with hnRNP A2 (DP3B3) and β-actin. The exogenous mutant hnRNP A2 (siR) resistant to si-A2#2 is indicated by an asterisk. The data are representative of three independent experiments. Error bars indicate the standard deviations of the means.

and calregulin, but not with GM130 and EEA1, at 24 h posttransfection (Fig. 4B and data not shown). We have shown previously that two amino acid residues (Gly^{42} and Pro^{43}) in the JEV core protein are responsible for nuclear localization (47). To further confirm whether the cytoplasmic localization of hnRNP A2 by the expression of JEV core protein is caused by active export from the nucleus or passive retention in the cytoplasm, FLAG-CoreM, which is defective in nuclear localization, was introduced into JEV-SGR-Huh7 cells. As shown in Fig. 4B, hnRNP A2 was also detected in the ER of the replicon cells transfected with FLAG-CoreM. We further examined the interaction of hnRNP A2 with the core protein by an immunoprecipitation analysis. Coprecipitation of hnRNP A2 with core protein, but not with calregulin, was observed in the JEV-infected 293T cells (Fig. 4C). Next, to confirm the role of the core protein in the replication of JEV, FLAG-Core was

Downloaded from http://jvi.asm.org/ on November 21, 2011 by Yoshiharu Matsuura